

Review

# From the Light Chain Sequence to the Tissue Microenvironment: Contribution of the Mesangial Cells to Glomerular Amyloidosis

Luis Del Pozo-Yauner <sup>1,\*</sup>, Elba A. Turbat-Herrera <sup>1,2</sup>, Julio I. Pérez-Carreón <sup>3</sup>  and Guillermo A. Herrera <sup>1,\*</sup>

<sup>1</sup> Department of Pathology, College of Medicine, University of South Alabama, Mobile, AL 36617, USA; etherrera@health.southalabama.edu

<sup>2</sup> Department of Pathology, Mitchell Cancer Institute, College of Medicine, University of South Alabama, Mobile, AL 36604, USA

<sup>3</sup> Laboratory of Liver Diseases, National Institute of Genomic Medicine, Tlalpan, Ciudad de Mexico 14610, Mexico; jjperez@inmegen.gob.mx

\* Correspondence: ldelpozoyauner@health.southalabama.edu (L.D.P.-Y.); gherrera@health.southalabama.edu (G.A.H.); Tel.: +251-470-5863 (L.D.P.-Y.); +251-471-7719 (G.A.H.)

**Abstract:** Studies carried out in the last three decades have significantly advanced our knowledge about the structural factors that drive the amyloid aggregation of the immunoglobulin light chains. Solid-state nuclear magnetic resonance and cryo-electron microscopy studies have resulted in huge progress in our knowledge about the AL fibril structure. Now, it is known that the assembly of the light chain into AL fibrils implies an extensive conformational rearrangement that converts the beta-sandwich fold of the protein into a near flat structure. On the other hand, there has also been significant progress made in understanding the role that some cell types play as facilitators of AL formation. Such a role has been studied in glomerular amyloidosis, where mesangial cells play an important role in the mechanism of AL deposition, as well as for the pathogenic mechanisms that result in glomerular/renal damage. This review addresses what we currently know about why and how certain light chains are prone to forming amyloid. It also summarizes the most recent publications on the structure of AL fibrils and analyzes the structural bases of this type of aggregate, including the origin of its structural diversity. Finally, the most relevant findings on the role of mesangial cells in the amyloid deposition of light chains in the glomerular space are summarized.

**Keywords:** light chain; amyloidosis; AL fibril; mesangial cell; protein aggregation; protein misfolding



**Citation:** Del Pozo-Yauner, L.; Turbat-Herrera, E.A.; Pérez-Carreón, J.I.; Herrera, G.A. From the Light Chain Sequence to the Tissue Microenvironment: Contribution of the Mesangial Cells to Glomerular Amyloidosis. *Hemato* **2022**, *3*, 232–267. <https://doi.org/10.3390/hemato3010019>

Academic Editors: Giovanni Palladini, Stefan Schönland and Laurent Garderet

Received: 2 January 2022

Accepted: 9 March 2022

Published: 17 March 2022

**Publisher's Note:** MDPI stays neutral with regard to jurisdictional claims in published maps and institutional affiliations.



**Copyright:** © 2022 by the authors. Licensee MDPI, Basel, Switzerland. This article is an open access article distributed under the terms and conditions of the Creative Commons Attribution (CC BY) license (<https://creativecommons.org/licenses/by/4.0/>).

## 1. Introduction

Proteins are key components of living organisms, since they are the molecules responsible for translating the information encoded in the cellular genome into the myriad of molecular actions that sustain life [1,2]. Such functional diversity is an expression of their structural diversity, unparalleled among the biomolecules. Many proteins acquire their functional capabilities through folding, a complex process that confers to the protein molecules a defined, generally compact, and stable tridimensional conformation known as the “native state” [3]. In contrast, there is a class of proteins, or protein segments, that lack a well-defined ordered structure at physiological conditions. This group is known as intrinsically disordered proteins (IDPs), and they account for around ~30% of the human proteome [4]. Upon binding to a functional partner, some IDPs undergo a disorder-to-order transition that results in a relatively compact and defined conformation [5]. Whether it occurs spontaneously or induced by the interaction with a functional partner, protein folding takes place in the highly crowded environment of the intracellular compartment, where each protein coexists with molecules of a very diverse chemical nature, including other proteins [6]. Hence, during the folding and after the native state has been adopted,

proteins face a constant risk of aggregation derived from spurious intermolecular contacts with other cellular components [7].

As part of their functional cycle in living cells, some proteins associate with each other, as well as with non-protein molecules, such as nucleic acids, to form liquid-like condensates that contain biomolecules in the absence of membrane structures [8]. Membrane-less condensates, such as nucleoli, stress granules, and processing (P) bodies, dynamically assemble and disassemble in a well-regulated manner, in response to cellular stress and other stimuli [8]. Disruption of the regulatory mechanisms that govern the formation and disassembling of these supramolecular complexes, as well as mutation of the constituent proteins, can lead to protein aggregation within phase-separated compartments, which has been linked to cancer [8,9] and neurodegenerative diseases [10]. On the other hand, proteins that are secreted into the extracellular compartment can misfold and aggregate in an unregulated manner, as a consequence of different environmental and protein-dependent factors [7]. This type of aggregation generally implies the loss of the normal function(s) of the involved protein, which in itself can put the viability of the living organism at risk if the lost function is critical for the life of the cell and cannot be replaced by other protein(s) [7,11]. Furthermore, protein aggregates are very toxic for cells, damaging them by different mechanisms [12–15]. Not surprisingly, the intrinsic propensity of proteins to aggregate has been one of the driving forces in their evolution, having left a mark in living organisms in the form of evolutionarily conserved mechanisms that work together to prevent protein aggregation [7,11,16–19]. Proteins have incorporated through evolution structural elements that protect them from aggregation. These elements inhibit aggregation through different mechanisms and structurally vary from a single charged residue placed at critical positions of the polypeptide chain to relatively complex folding motifs adopted by a specific protein segment [20–23]. Moreover, associating into stable quaternary complexes is also an effective strategy to protect proteins from aggregation [24–26]. In addition to these protein-specific strategies, living organisms have developed complex intracellular and extracellular mechanisms for dealing with protein aggregation [27,28]. In general, these mechanisms work by funneling the protein molecules into the native folding pathway, avoiding the events that can cause them to aggregate, or by removing the proteins that have suffered structural damage and are at risk of aggregating, or have already aggregated [29]. Although highly effective, the strategies used by nature to avoid protein aggregation are far from infallible. There are many circumstances in which, despite the aforementioned mechanisms, proteins misfold and aggregate, causing disease [7]. Protein can form different types of pathological aggregates, which differ from each other by their physicochemical and biological properties, a reflection of their differences in internal structure [30]. One of them is amyloid, which is associated with the pathogenesis of a clinically heterogeneous group of diseases, collectively known as amyloidosis [31]. Amyloid is characterized by fibrillar morphology at electron microscopy level, and the ability to bind Congo red and thioflavin T (ThT). When stained with Congo red and observed under a polarized light microscope, amyloid, irrespective of its chemical composition, yields an optical phenomenon known as birefringence that, although usually described as apple-green, can also be yellow, orange, or red [32,33]. This property is used to detect tissue amyloid deposition in clinical practice. Another property of amyloid used for clinical diagnosis [34,35], as well as for research, is the ability to bind ThT and yield a fluorescence with a  $\lambda_{\max}$  of around 482 nm, when excited at 450 nm [36,37]. Structurally, the amyloid's hallmark is a cross- $\beta$  core formed by intermolecular  $\beta$ -sheets that run along the fibril's axis [38]. Currently, thirty-six different proteins and peptides are known to form amyloid in humans [39]. Depending on the number of organs affected, amyloidoses are classified as localized or systemic [31]. The most frequently diagnosed systemic amyloidosis in Western countries is AL amyloidosis, a disease caused by the misfolding and amyloid deposition of a monoclonal immunoglobulin light chain (LC) [40]. The exact incidence of AL amyloidosis is unknown. It has been estimated in the range of 10 to 12 cases per million person-years, depending on the population and the method used to calculate the parameter [41–45]. A recent study that used claim

data found that the prevalence of AL amyloidosis in the United States increased from 15.5 cases per million in 2007 to 40.5 in 2015, which means an annual percentage change of 12%. The incidence ranged from 9.7 to 14.0 cases per million person-years, with no statistically significant increase. The authors estimated that there are at least 12,000 adults in the United States living with AL amyloidosis [46].

## 2. Genetic and Structural Characteristics of the Immunoglobulin LCs

The immunoglobulin LCs, as its name indicates, are one of the two subunits that compose the antibodies. They are 215–225 amino acids in length and fold into two domains, the variable ( $V_L$ ) and the constant ( $C_L$ ) domains, both having the characteristic immunoglobulin fold (Figure 1A) [47]. The immunoglobulin fold is composed of two anti-parallel  $\beta$ -sheets with a Greek key topology, which associate face-to-face to form a two-layer sandwich [47]. The LCs are encoded by three different gene segments, two for the  $V_L$  domain, known as variable and joining gene segments, and the constant domain gene segment for the  $C_L$  domain. These genetic elements are dispersed in the human genome but end up fused into a functional LC gene through the mechanism of  $V_L$ - $J_L$ - $C_L$  combinatorial recombination that takes place during the ontogenesis of the B-lymphocytes, helping to generate a diverse repertoire of antibodies (Figure 1B). According to the sequence of the  $C_L$ , LCs are classified into two types, kappa ( $\kappa$ ) and lambda ( $\lambda$ ). The sequence of the  $V_L$  is used to subdivide the LCs into six  $\kappa$  ( $\kappa 1$  to  $\kappa 6$ ) and ten  $\lambda$  ( $\lambda 1$  to  $\lambda 10$ )  $V_L$  subgroups ([http://www.imgt.org/IMG\\_Trepertoire/](http://www.imgt.org/IMG_Trepertoire/); data accessed on 2 January 2022). The  $V_L$  subgroups were initially established on the basis of both protein sequence similarity and antibody specificity [48], but now it is known that they represent LCs encoded by groups of phylogenetically closely related  $V_L$  gene segments that were generated in relatively recent events of gene duplication and divergence [49]. The number of  $V_L$  gene segments per  $V_L$  subgroup varies from only one, as is the case for the subgroup  $\lambda 6$ , to twenty in the case of the subgroup  $\kappa 1$  [50,51].

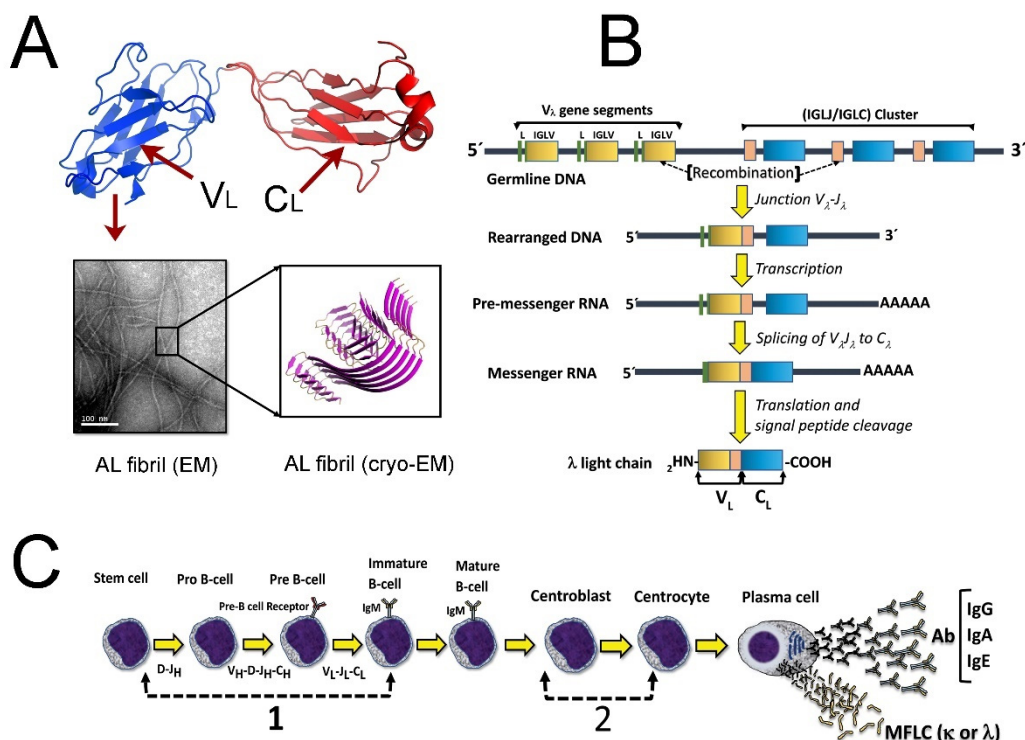


**Figure 1.** Cellular and molecular events related to immunoglobulin LC amyloid aggregation. (A) Structural characteristics of the immunoglobulin LCs and AL amyloid fibrils. The LC structure shown is that of the full-length  $\lambda$  LC MCG determined by X-ray crystallography (PDB 3MCG). The variable ( $V_L$ ) and constant ( $C_L$ ) domains are colored in blue and red, respectively. Electron

microscopy (EM) image of amyloid-like fibrils formed by the  $\lambda 6$  rV<sub>L</sub> protein 6aJL2. Cryo-EM structure of ex vivo  $\lambda 6$  AL fibrils obtained from the cardiac deposits in a patient with AL amyloidosis (PDB 6HUD). The core of the AL fibrils is composed only by segments of the V<sub>L</sub> domain. (B) Schematic representation of the rearrangement of the V<sub>L</sub> (IGLV), J<sub>L</sub> (IGLJ), and C<sub>L</sub> (IGLC) gene segments of  $\lambda$  LCs. The gene segments' rearrangement is completed by means of somatic recombination. Note that the V<sub>L</sub> domain of the LC is encoded by the IGLV and IGLJ gene segments, while the C<sub>L</sub> domain is encoded by the IGLC genes. (C) B-cell differentiation pathway and the mechanisms for the generation of antibody diversity. The repertoire of polyclonal antibodies is generated in two key molecular events: (1) rearrangement of the heavy (V<sub>H</sub>, D, J<sub>H</sub>, and C<sub>H</sub>) and LC (V<sub>L</sub>, J<sub>L</sub>, and C<sub>L</sub>) gene segments, and (2) somatic hypermutation, which occurs at specific stages of B-cell differentiation. The rearrangement of the immunoglobulin gene segments occurs prior to the activation of the B-lymphocyte by antigen (antigen-independent process), while the somatic mutation occurs in centroblast cells and is an antigen-dependent mechanism. Plasma cells, the final stage of B-cell differentiation, secrete large amounts of the specific antibody (IgG, IgA, or IgE) for the production of which the plasma cell clone was genetically programmed during ontogenesis. Under certain circumstances, a clone of plasma cells can overproduce the antibody LC and secrete it in a free state, which entails the risk of aggregation and disease. MFLC stands for monoclonal free light chain.

### 3. Structural Factors and Environmental Conditions That Drive the Amyloid Aggregation of the LCs

AL amyloidosis is a monoclonal gammopathy in which an abnormally proliferating, but usually small [52], plasma cell clone overproduces a misfolding-prone, structurally homogeneous LC that is secreted into the bloodstream in a free state (Figure 1C) [53]. This means that the monoclonal free LC circulates in the body fluid deprived of the protection provided by the quaternary structure of the antibody. Such protection comes in the form of stabilizing contacts with the heavy chain (HC) that decreases the probability of misfolding [54,55]. Moreover, a stable LC–HC interface also renders potentially aggregation-prone segments of the LC less accessible to intermolecular interactions that may nucleate aggregation. However, it is important to note that a fraction of monoclonal gammopathy patients with a circulating monoclonal LC never present signs or symptoms of AL amyloidosis, even after a long period of clinical evaluation [56,57]. This suggests that, although the presence of a circulating monoclonal free LC is a requirement, it is not sufficient for the amyloid aggregation to occur. The evidence supports the notion that it is the interplay between the structural and physicochemical properties of the circulating monoclonal LC and a series of patient-specific factors, some of which are still not well understood, that ultimately determines whether a LC will deposit as amyloid fibrils [58–60].

#### 3.1. Pro-Fibrillogenic Sequences in LCs

So far, thirty-six different proteins and peptides have been identified as amyloid precursors [39]. While they all share the ability to self-assemble into ordered fibrillar aggregates with a group of common structural and physicochemical properties, it is remarkable that they do not share significant similarity in sequence or tridimensional structure. This, and the observations that fibrils with the properties of amyloid can be formed by polyaminoacids [61], as well as short peptides without stable globular folds [62–64], led researchers to deduce that the amyloid fibril represents a generic conformational state of the polypeptide chain, different from the globular folding adopted by most proteins in physiological condition. According to this notion, the main force driving the assembly of peptides and proteins in amyloid fibrils would be the intrinsic propensity of the polypeptide backbone to assemble into periodic structures [65]. However, experimental data also show that the sequence of the amyloidogenic protein or peptide modulates the kinetics and thermodynamics of the fibril formation, as well as the structural and biophysical properties of the aggregates, such as morphology, cytotoxicity, stability and efficiency for seeding the fibrillogenesis [62,66]. Studies based on libraries of short synthetic peptides

identified sequence patterns compatible with amyloid-like structures [67,68]. In addition, it was demonstrated that the ability to form amyloid-like fibrils can be transferred from one amyloidogenic protein to another not amyloidogenic one by grafting into the second of the amyloid-forming segments taken from the former [69–71]. These and other studies led Esteras-Chopo et al. to postulate that the ability of a protein to form amyloid fibrils is contained in short stretches of its sequence, known as pro-amyloidogenic hotspots. This statement is known as the “amyloid stretch hypothesis” [69,72]. It is believed that the pro-amyloidogenic hotspots drive, in a sequence-dependent manner, the self-assembly of the protein or peptide into the ordered structure of the amyloid fibrils [69,72]. An attribute of the pro-amyloidogenic hotspots is the ability to form amyloid-like fibrils when assayed as isolated peptides [64]. Studies based on X-ray diffraction of micro crystals formed by short peptides that also form amyloid-like fibrils provided a structural explanation of the relationship between sequence and fibril-forming capability. Amyloid-forming peptides were found to adopt an extended  $\beta$  conformation and associate side by side in the crystal lattice, either in a parallel or antiparallel arrangement. This results in intermolecular beta sheets that extend along the longitudinal axis of the fibrous crystal. The  $\beta$ -sheets stack on top of each other in a lamellar structure, stabilized by the tight interdigitation of the amino acid side chains oriented to the sheets interface. This arrangement is known as the “steric zipper” [73–76]. Consequently, it was suggested that the pro-amyloidogenic hotspots are those sequence stretches of a protein capable of associating into a stable steric zipper [76]. The key role attributed to these protein segments in the mechanism of amyloidogenesis makes them obvious targets for therapeutic strategies aimed at inhibiting amyloid aggregation [77–79]. Therefore, there is much interest in identifying pro-amyloidogenic hotspots in proteins that are related to pathological amyloid deposition, such as LCs.

The identification and characterization of pro-amyloidogenic sequences in LCs have been addressed by some laboratories. Brumshtein et al. used a strategy based on the theoretical prediction of steric zipper-forming sequences with the computational algorithm ZyperDB [80] and site-directed mutagenesis for identifying amyloid-driving segments in both  $\kappa$  and  $\lambda$  LCs [81]. This approach led to the identification two distinct segments shared by both LC types that, by means of X-ray crystallographic analysis, were shown to form self-complementary steric zippers. Since point mutations of conserved residues of these segments by proline (Pro) inhibited the fibrillogenesis of the intact  $V_L$  domain, it was concluded that they can independently drive the amyloid aggregation of the LC through their ability to form a self-complementary steric zipper [81].

Schmidt et al. also used prediction algorithms, in combination with several biophysical and structural methods, to search for pro-amyloidogenic sequences in a  $\lambda$  LC derived from an AL patient [82]. They identified a fibrillogenic fragment spanning part of the complementarity determining regions 1 (CDR1) and the  $\beta$ -strand C that formed amyloid-like fibrils. Using cryo-electron microscopy (cryo-EM), it was determined that the fibrillar peptide arranged in a lattice-like assembly of face-to-face packed peptide dimers that resembles the self-complementary steric zippers observed in fibrous crystals [82].

Recently, Ruiz-Zamora et al. reported several pro-amyloidogenic hotspots dispersed along the sequence of the  $\lambda 6 V_L$  protein 6aJL2 [75]. This protein is encoded by the germline  $V_L$  gene segment *IGLV6-57*, which is associated with AL amyloidosis [83]. Ruiz-Zamora et al. used two complementary strategies to increase the probability to identify amyloid-forming segments in 6aJL2 protein. One strategy consisted of the theoretical prediction of amyloid-forming sequences by several web-based computational algorithms, and the validation of the prediction with libraries of synthetic peptides. The second strategy was based on the proteolysis of the 6aJL2 protein with trypsin, seeking to generate peptide fragments capable of forming amyloid-like fibrils, indicative of the presence of pro-fibrillogenic sequences. This approach was combined with the analysis of libraries of synthetic peptides designed for a more accurate characterization of the protein fragments generated by proteolysis. In both strategies, several physicochemical and structural techniques were used to characterize the protein fragments and the aggregates. By combining these two strategies,

Ruiz-Zamora et al. identified three large fibril-forming fragments of 6aJL2 protein that, in conjunction, span 60% of the protein sequence (Figure 2A) [84]. One of the fibrillogenic fragments identified in this study was composed by two peptide fragments linked by the conserved intradomain disulfide bond Cys23-Cys88 (Figure 2A). It was shown that the aggregation of this fragment depends on the preservation of the disulfide bond Cys23-Cys88, a feature that could be a reminiscence of the structural restrictions that operate in the aggregation of the intact V<sub>L</sub> domain [75]. Interestingly, the most aggregation-prone fragment of 6aJL2 protein is that spanning from Ser26 to Arg29, a segment that comprises the CDR1 and the β-strand C (Figure 2A). This highly amyloidogenic fragment is structurally homologous to that reported by Schmidt et al. [82]. Remarkably, several other germline κ and λ V<sub>L</sub> genes also encode a pro-amyloidogenic hotspots for the CDR1, which suggests that this loop plays an important role in the mechanism of LC amyloid aggregation [75].

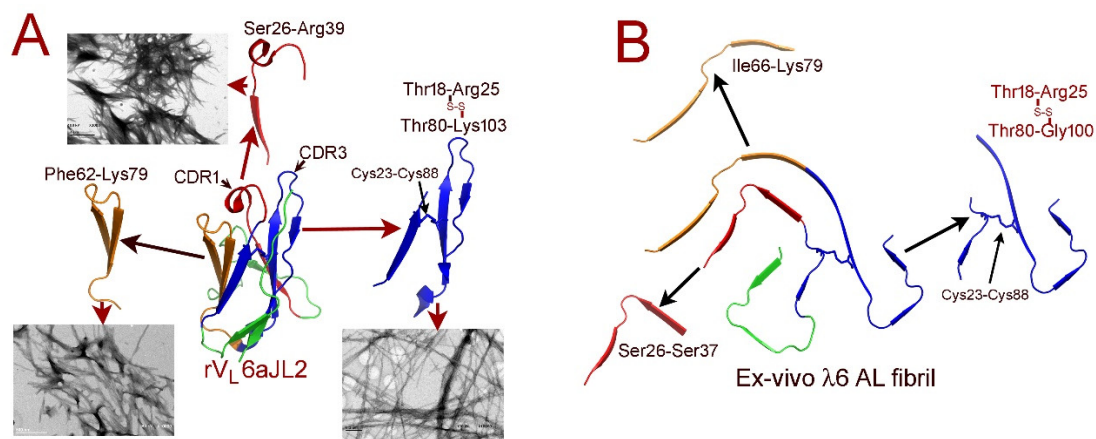


**Figure 2.** Fibrillogenic fragments of the λ6 germline-encoded rV<sub>L</sub> protein 6aJL2. (A) Location in the tridimensional structure of 6aJL2 protein of the three main fibrillogenic fragments generated by limited proteolysis with trypsin, as described in [75]. The N- and C-terminal residues in each fragment are indicated, using the same numbering of the protein. The inserts show an electron microscopy micrograph of the amyloid-like fibrils formed by each fragment, analyzed by negative staining. For reference, the complementarity determining regions (CDRs) 1 to 3 are indicated (B) Location in the tridimensional structure of the ex vivo AL fibril AL55 of the fibrillogenic fragments identified in the rV<sub>L</sub> protein 6aJL2. The fibril AL55 was obtained from the deposits of a patient with cardiac AL amyloidosis and was formed by the λ6 LC [85]. The partial overlap of the fibrillogenic fragments of 6aJL2 protein with the segments that form the β-core of the ex vivo AL fibril AL55 supports the hypothesis that sequences contained within them also drive the in vivo aggregation of λ6 light chains. The conserved intradomain disulfide bond between cysteines 23 and 88 (Cys23-Cys88) are represented in stick format in both the 6aJL2 protein and the AL55 fibril. The structure of the rV<sub>L</sub> 6aJL2 and the AL fibril AL55 was determined by X-ray crystallography (PDB 2W0K) and cryo-EM (PDB 6HUD), respectively. The images of both structures were created with PyMOL.

One contribution from the study of Ruiz-Zamora et al. that is worth mentioning is the validation of a proteolysis-based strategy that allowed the identification of amyloid-forming protein fragments longer than those usually yielded by prediction-based approaches. Such a result was made possible because the search strategy designed by Ruiz-Zamora et al. was based on the concept that the pro-amyloidogenic hotspots of globular proteins consist of relatively long regions of the molecule that are flanked by gatekeeper residues (Arg, Lys, Glu, Asp, and Pro) [20,21], which drive amyloid aggregation by means of the cooperative interaction of short aggregation-prone stretches contained in the long pro-amyloidogenic hotspots [86] (Figure 2A,B). Another contribution, derived from the aforementioned study, established that V<sub>L</sub> 6aJL2 contains several long amyloid-forming segments that, together, comprise more than 60% of its sequence (Figure 2A). This finding led to the hypothesis that the core of the amyloid-like fibrils formed by the model protein 6aJL2, as well as by the LCs

derived from the  $V_L$  gene segment *IGLV6-57*, should be made up of several segments of the protein in  $\beta$  conformation (Figure 2B). An implication of this hypothesis is that the assembly of the protein into amyloid-like fibril would require an extensive conformational change, with the consequent loss of its native folding. Structural studies carried out subsequently support this hypothesis [85,87].

### 3.2. The Folding Stability and Role of the Somatic Mutations

A large amount of data obtained through more than four decades of research identify the thermodynamic stability of the native folding as a major driver of the amyloid aggregation of the LCs [88–103]. Overall, the amyloidogenic LCs tend to be thermodynamically less stable than the non-pathogenic ones [90]. It has been postulated that the decrease in folding stability makes the LC more prone to adopt non-native conformations that may have propensity to aggregate. This concept is at the core of the paradigm of non-native intermediaries as key components of the LC amyloid aggregation pathway, and is essential for the comprehension of AL amyloidosis as a misfolding disease [54,88,92,104,105]. The decreased folding stability that characterizes amyloidogenic LCs is primarily the consequence of the somatic mutations. These changes are introduced mostly in  $V_L$  during the affinity maturation of the antibody in response to a specific antigen [54,60,88,93,95,97,98,106]. Moreover, as will be discussed in another part of this review, the structural characteristics of the germline  $V_L$  protein from which a particular LC derives also appear to contribute to determining its folding thermodynamic and aggregation propensity. Some germline  $V_L$  proteins are relatively unstable and misfolding-prone proteins, which may confer risk of misfolding and aggregation to the light chains derived from them [107].

In addition to compromising the LC folding stability, the somatic mutations can promote amyloid aggregation through other mechanisms [54]. Some mutations promote aggregation by destabilizing the non-covalent dimer that some LCs tend to form [108–110]. This deprives the LC from the stabilizing contacts at the LC–LC dimer interface, which, as a reminiscence of the LC–HC interface, also protects LC from aggregation [55,111]. Other mutations modify the charge distribution and polarity of the protein surface, increasing the intrinsic aggregation propensity [100]. Studies suggest that some mutations promote aggregation by disrupting the dynamic of specific segments of the protein, increasing their conformational flexibility. Such an effect can promote amyloid aggregation, even if it is not accompanied by a decrease in the protein folding stability [112–114]. Mutations can also disrupt the structural elements that protect LCs from aggregation [22], a topic that will be addressed in more detail in another part of this review. Furthermore, mutations can modulate the kinetics of unfolding/refolding of LCs, increasing, in some environmental conditions, the fraction of molecules that populate aggregation-prone misfolded intermediates [93]. Given that, on average, the  $V_L$  of an amyloidogenic LC has 8–12 somatic mutations, the increased aggregation propensity that characterizes these proteins is likely due to the effects of several mutations acting through more than one mechanism.

### 3.3. Contribution of the $V_L$ Gene Segment to the Propensity of the LCs to Form Amyloid

On average, the  $\kappa:\lambda$  ratio in the normal repertoire of polyclonal antibody is  $\sim 2:1$ . In contrast, the  $\lambda$  isotype widely exceeds  $\kappa$  among amyloidogenic LCs, with the  $\kappa:\lambda$  ratio being 1:3 [115,116]. Such a difference is mostly determined by the strong association of a group of  $\lambda V_L$  gene segments with amyloidosis. Nearly 40 years ago, Solomon et al. reported the preferential association of LCs of the  $\lambda 6 V_L$  subgroup with AL amyloidosis [117]. This finding was corroborated in a subsequent study in 1992, carried out in a larger series of AL patients [118]. In both studies, the AL proteins were classified with an immunoassay with a set of anti- $V_L$  subgroup-specific antibodies. Therefore, the frequency of usage of the  $V_L$  gene segments in those AL patients was not determined. More recently, studies based on DNA sequencing revealed that the use of the  $V_L$  gene segments among amyloidogenic LCs differs from that characterizing the normal repertoire of polyclonal antibodies [119–122]. Only five gene segments, four  $\lambda$  (*IGLV1-44*, *IGLV2-14*, *IGLV3-1*, and *IGLV6-57*) and one  $\kappa$

(*IGKV1-33*), account for ~60% of the amyloidogenic LCs compiled in the AL-Base database ([https://wwwapp.bumc.bu.edu/BEDAC\\_ALBase](https://wwwapp.bumc.bu.edu/BEDAC_ALBase); data accessed on 2 January 2022) [115]. This is remarkable, considering that they represent only ~7% of the human repertoire of  $V_L$  genes, composed of 74 elements (<http://www.imgt.org/IMGTrepertoire/>; data accessed on 1 January 2022). The determinants of such a skewed repertoire of  $V_L$  gene segments in AL amyloidosis remain unknown. It was initially suggested that the association of the aforementioned five  $V_L$  gene segments with amyloidosis could be determined by the biophysical and structural properties of the protein encoded by their germline sequence [83]. According to this hypothesis, the AL-associated  $V_L$  genes encode germline  $V_L$  proteins intrinsically prone to misfolding and aggregate as amyloid fibrils. Accordingly, the association of LCs derived from these  $V_L$  genes with AL amyloidosis would reflect the amyloid-forming capability inherited from the germline  $V_L$  proteins. To test this hypothesis, Garay et al. evaluated the thermodynamic stability and in vitro fibrillogenesis of recombinant (r)  $V_L$  proteins with the germline sequence of the gene segments *IGLV1-44*, *IGLV2-14*, *IGLV6-57* and *IGKV1-33* [107]. It was found that the germline  $V_L$  proteins encoded by the AL-associated  $V_L$  gene segments differ broadly in thermodynamic stability and aggregation propensity [107]. While the germline  $V_L$  protein encoded by *IGLV6-57* ( $\lambda 6$ ) was found to be prone to misfolding and readily formed amyloid-like fibrils, those encoded by *IGLV1-44* ( $\lambda 1$ ) and *IGKV1-33* ( $\kappa 1$ ) were thermodynamically stable and barely aggregated in vitro [107]. Therefore, it was concluded that the association of this group of  $V_L$  genes with amyloidosis cannot be totally explained by the folding thermodynamic and amyloid-forming capability of the germline  $V_L$  proteins they encode [107]. It is worth noting that *IGLV6-57* encodes ~20% of AL of  $\lambda$  type [121], but it is expressed only in 2% of the normal polyclonal bone marrow B cells expressing a  $\lambda$  LC [122]. More strikingly, with only one well-documented exception [102,123], all monoclonal  $\lambda 6$  LCs so far identified in monoclonal gammopathies have been shown to be implicated in amyloid deposition [107,115]. In conjunction, these data support the notion that, in addition to factors such as the somatic mutations, post-translational modifications (PTMs), and organ-specific variables, the germline  $V_L$  protein encoded by *IGLV6-57* contribute in some extent to make the  $\lambda 6$  LCs high propense to aggregate as amyloid in vivo [107]. In contrast, the germline  $V_L$  appears to play a minor role in the association of the LCs encoded by *IGLV1-44* and *IGKV1-33* to amyloidosis [107].

On the other hand, it has been speculated that the skewed repertoire of  $V_L$  gene segments in AL amyloidosis results from distortions in the regulatory mechanisms of the antibody repertoire diversification, causing changes in the accessibility of certain  $V_L$  gene segments to recombination events [119]. Furthermore, it has been suggested that the overrepresentation of some  $V_L$  genes in AL amyloidosis may reflect the preferential selection and expansion of B cell clones expressing certain  $V_L$  gene segments by an antigen-dependent mechanisms [119]. It is worth mentioning that marked differences in the usage of the  $V_L$  gene repertoire between localized and systemic AL amyloidosis [121] and between IgM and non-IgM AL amyloidosis [124] have been reported. An example of this is the gene segment *IGLV6-57*, which accounts for ~22% of the amyloidogenic  $\lambda$  LCs in systemic amyloidosis, but only accounts for 10% of the cases of localized  $\lambda$  amyloidosis [121]. The frequency of this gene segment was also found to differ significantly between non-IgM and IgM AL amyloidosis cases. It caused approximately 18% of non-IgM AL  $\lambda$  cases, but only 2% of those classified as IgM AL  $\lambda$  [124]. The last figure is similar to the frequency determined for *IGLV6-57* in the normal repertoire of LCs in bone marrow B cells [122]. This means that *IGLV6-57* is overrepresented in some, but not all forms of AL amyloidosis.

In conjunction, these studies are consistent with the notion that the probability for a  $V_L$  gene segment to be involved in AL amyloidosis depends on both genetic and environmental factors. The origin of the amyloidogenic plasma cell clone and the characteristics of the microenvironment where it expands and secretes the LC appear to play a role.

The  $V_L$  gene segment encoding the amyloidogenic LC can also confer it organ tropism [119–121,125]. It has consistently been found that renal involvement is more common in AL patients with a LC derived from *IGLV6-57* compared with those with a dif-

ferent LC [119–121,125]. Cardiac involvement, a clinical condition that deeply impacts the survival of AL patients, has been found to be more frequent in patients with a LC encoded by *LV1-44* ( $\lambda$ 1). This clinical condition is also frequent in AL patients with LCs encoded by the gene segments *IGLV3-19* ( $\lambda$ 3) and *IGKV1-05* ( $\kappa$ 1), although their frequency in AL amyloidosis is low. The gene segments *IGLV2-14* ( $\lambda$ 2) and *IGKV1-33* ( $\lambda$ 3) have been associated with a higher rate of peripheral neuropathy and liver involvement, respectively [121].

### 3.4. How Does the LC Protect Itself from Aggregation?

As with other proteins with a high content of  $\beta$  structures, LCs are at risk of aggregation if the  $\beta$  strands placed at the edges of the  $\beta$  sandwich, or any other segment of the molecule with an aggregation-prone sequence, are left exposed to intermolecular interactions [22]. To deal with this risk, LCs have incorporated several structural elements that protect the edge strands from edge-to-edge interactions, an evolution-driven strategy that has been called “negative design” [22]. At least three different protective structural elements are shared by all  $V_L$  domains, irrespective of if they are  $\kappa$  or  $\lambda$ . They are the sheet-switch motif and  $\beta$ -bulge of the  $\beta$ -strands A and G, respectively, and the long loop spanning positions 40 to 60, henceforth loop 40–60 (Figure 3). The sheet-switch motif of the  $\beta$ -strand A is characterized by an abrupt kink in the polypeptide chain encompassing residues 7–8 in  $\lambda$ , or 8–9 in  $\kappa$  LCs. In  $\lambda$  LCs, a Pro residue may be present at position 7 or 8, or in both, while in  $\kappa$  proteins, Pro is only found at position 9. Structurally speaking, the sheet-switch breaks the  $\beta$ -strand A into two halves. The N-terminal half interacts by H-bonding with the  $\beta$ -strand B, integrating into the  $\beta$ -sheet formed by strands B-E-D. The C-terminal half integrates into the other  $\beta$ -sheet of the sandwich (strands C-F-G) by H-bonding with the  $\beta$ -strand G (Figure 3A). Therefore, the  $\beta$ -strand A covers the longer strands B and G with segments, respectively, that are too short to sustain stable edge-to-edge interactions [22]. Additionally, Pro residues located in the kink region physically hinder the access to both edges, further helping to prevent aggregation [22]. The  $\beta$ -bulge is described as a region between two consecutive  $\beta$ -type hydrogen bonds which includes two residues on one strand opposite a single residue on the other strand, an arrangement that introduces a bend in the  $\beta$ -sheet [126] (Figure 3B). The  $\beta$ -bulge of the strand G is encoded by the LC joining gene segment (*IGVJ*), and structurally is centered on the residue at position 100. The germline-encoded residue at this position varies, depending on the *IGVJ* allele. It is Gln, Pro, or Gly in  $\kappa$  LCs and Gly, Thr, Ser, or Glu in  $\lambda$  LCs. However, in both  $\kappa$  and  $\lambda$  LC, residues at positions 99 and 101 are two conserved Gly ([http://www.imgt.org/IMG\\_Trepertoire/LocusGenes/#F](http://www.imgt.org/IMG_Trepertoire/LocusGenes/#F); data accessed on 2 January 2022). It is thought that the  $\beta$ -bulge inhibits aggregation by physically blocking access to the edge strand G (Figure 3B). The third protective structural element common to all  $V_L$ , the loop 40–60, covers the edge strands C and D, preventing them from engaging in edge-to-edge contacts (Figure 3C) [22]. The loop 40–60 comprises the CDR2 and, in the intact antibody, participates in the  $V_H$ – $V_L$  interface. In free LCs, it forms part of the  $V_L$ – $V_L$  interface formed in LC dimers. Depending on the LC, the loop 40–60 contains three or four relatively conserved Pro residues that likely provide it with conformational stability, thereby contributing to its protective function. (Figure 3C).

Since the aforementioned structural elements are part of the evolutionarily selected mechanisms to prevent aggregation in LCs, it is rational to anticipate that conformational changes that undermine their protective function are an essential component of the mechanism of LC amyloid aggregation, likely as triggering events of the aggregation. Structural changes can be caused by destabilizing somatic mutations, and/or PTM, such as the oxidation of certain side chains, aberrant proteolysis, or glycosylation [95,98,106,109,112–114,127–131]. Additionally, variation in the local environment of pH, ionic strength, or temperature can exert similar effects [99,104,132–134].

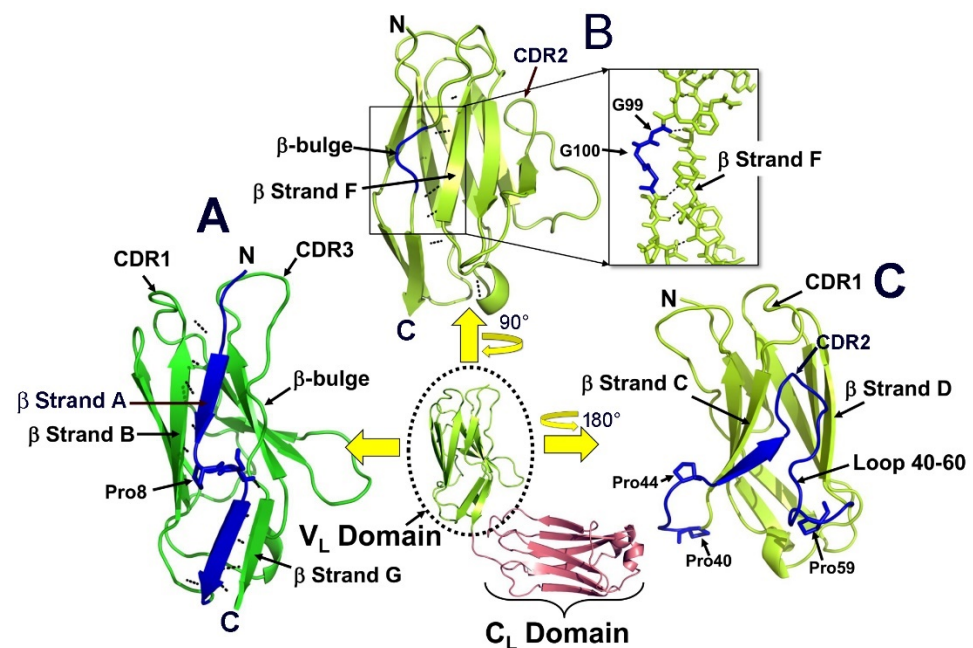


**Figure 3.** Structural elements of the  $V_L$  domain that prevent edge-to-edge aggregation. (A) Sheet-switch motif of the  $\beta$ -strand A, (B)  $\beta$ -bulge of the  $\beta$ -strand G, and (C) loop 40–60. The three mentioned structural elements are indicated in the figures and highlighted in blue. The  $\beta$ -strands B, D, C, and G are edges of the  $\beta$ -sheets of the domain. In A and B, the H-bonds between adjacent strands are represented as black dotted lines. The insert in B shows the structural relationship of the  $\beta$ -bulge in strand G with amino acid residues of strand F. The glycine residues at positions 99 and 100 (G99 and G100) are indicated. For reference, the CDRs 1 to 3, the structurally relevant proline (Pro) residues, and the N- and C-terminal of the  $V_L$  domain are indicated. The image of the full-length LC and the  $V_L$  domains correspond to the crystallography structure of the  $\kappa 1$  LC DEL (PDB 1B6D) and were prepared with PyMOL.

A study based on sequence analysis of more than one hundred amyloidogenic LCs found that the loop 40–60 are frequently targeted by non-conservative somatic mutations in both  $\kappa$  and  $\lambda$  AL [98]. As a trend, AL LCs bear a higher number of non-conservative mutations in positions of the loop 40–60 than the non-pathogenic LCs, or the group of LC from multiple myeloma patients [98]. Moreover, a high number of non-conservative mutations were also found in  $\beta$ -strands A and G in all AL sequences; with  $\beta$ -strand G bearing more non-conservative mutations in the  $\lambda 6$  sequences [98]. Remarkable, a statistically significant difference in the number of non-conservative mutations in the  $\beta$ -strand A was found among AL patients classified by the level of involved serum free LC (iFLC) at diagnosis. Those patients with a lower level of iFLC had a higher number of non-conservative mutations in the  $\beta$ -strand A [98]. This finding agrees with in vitro studies that have shown that mutations targeting structural residues at the  $\beta$ -strand A of the  $V_L$ , as Pro residues located in the kink are particularly effective in promoting LC amyloid aggregation [94,127]. Although without reaching statistical significance, the number of non-conservative mutations in  $\beta$ -strand B, as well as in positions of loop 40–60, was also higher in AL patients with low iFLC [98]. It is important to highlight that the authors of this study interpreted the low level of iFLC as expression of a more aggregation-prone LC [98].

There is experimental evidence suggesting that  $V_L$  structural elements with a protective role are involved in the conformational adjustments that trigger aggregation. Mukherjee et al. carried out NMR analysis of the  $\kappa 4$  r $V_L$  protein Len at pH 2.0, a condition shown to promote the aggregation of the protein as amyloid-like fibrils. The analysis revealed three contiguous segments of about 5–20 residues that displayed increased conformational flexibility [135]. These segments encompassed residues Val3 to Asp9 ( $\beta$ -strand A), Gln37 to Val58 (loop 40–60), and Gln89 to Gln100 (CDR3 and strand G) [135]. They concluded that

the group of amino acids with high conformational flexibility at pH 2 are involved in the earliest stages of Len misfolding [135].

In addition to the aforementioned protective structural elements, LCs also use other mechanisms to prevent aggregation, which vary from one protein to another, depending on the encoding IGVL and IGVJ gene segments. Placing the large and charged amino acids Arg and Lys in strategic positions at the edge strands, or, as was mentioned above, placing Pro residues at positions where they stabilize protective motifs and hinder the access to aggregation-prone segments are other protective strategies used by LCs to prevent aggregation [22]. Another anti-aggregation strategy identified in LCs is the folding of pro-amyloidogenic segments into helices, despite the intrinsic propensity of these sequences to adopt  $\beta$  conformation [136]. The CDR1 of the  $\lambda 6$  LCs is an illustrative example of this strategy. As mentioned in previous sections, the CDR1 in  $\lambda 6$  LCs is part of a pro-amyloidogenic hotspot [75] (Figure 2A). The native fold of this loop comprises an helical segment in its C-terminal half, a type of folding that results from structural constraints imposed by other segments of the domain [137]. Such helical folding allows the CDR1 to be exposed at the LC surface, a critical requirement for its function as a recognition loop, which at the same time avoids the risk of aggregation by  $\beta$ - $\beta$  interaction. This strategy is also used by the LCs of the  $\lambda 1$  and  $\lambda 2$  subgroups, in whose CDR1 the presence of pro-amyloidogenic hotspots has also been demonstrated [75,82]. In a recent study, Peterle et al. found evidence that a conservative mutation in the CDR1 of an AL  $\lambda 6$  LC promoted amyloid aggregation by increasing the conformational flexibility of the loop, an effect that propagated to other regions of the domain [113]. A more flexible CDR1 would be more prone to undergoing the transition from  $\alpha$ -helix to  $\beta$ -strand that, as will be seen elsewhere in this review, is an integral part of the amyloid aggregation mechanism of  $\lambda 6$  LCs [85,87].

In conjunction, these studies support the notion that conformational changes at structural elements of the  $V_L$  with protective function, such as  $\beta$ -strands A and G, loop 40–60, and CDR1, are early events of the mechanism of LC amyloid aggregation.

### 3.5. Intact LC as the AL Precursor and the Role of Proteolysis

It has long been known that the most abundant component of the AL deposits are fragments of the monoclonal LC comprising the  $V_L$  alone, or this domain plus a variable portion of the  $C_L$ , although the intact LC may also be present. This observation, and evidence obtained in animal models [138], led researchers to infer that the structural factors that make LCs amyloidogenic are contained in the  $V_L$  sequence. As a consequence, the use of recombinant  $rV_L$  proteins as experimental models to study the mechanism of LC amyloid aggregation was adopted by several laboratories [83,91,96,102,108,139]. Studies based on these proteins contributed importantly to the understanding of the mechanism of LC misfolding and aggregation, as well as in identifying structural factors that make the LC amyloidogenic [75,83,94,101,102,104,108,109,127,132,133,140–144]. However, the precursor of the AL is the intact monoclonal LC, a fact that should be considered when interpreting the results of studies carried out with  $rV_L$  models. The  $C_L$  profoundly influences the thermodynamic stability and aggregation propensity of the LC [145]. As a rule, full-length LCs exhibit significantly slower fibrillogenesis kinetics than their respective  $V_L$ , and in some cases, they do not aggregate at all [55,146]. Such differences in aggregation propensity likely reflect the higher stability of the LC compared to the  $V_L$  [55,145]. LCs tend to form extensive  $V_L$ - $V_L$  and  $C_L$ - $C_L$  interfaces that result in more stable dimers than those formed by  $V_L$  proteins, which inhibits aggregation [55]. Additionally, many LCs feature a kinetically controlled and irreversible thermal unfolding reaction, even if this process is partially reversible for their constituent domains,  $V_L$  and  $C_L$  [145,146]. This phenomenon, which has been related to restrictions imposed by cis/trans isomerization of Pro residues at the  $C_L$ , may prevent some LCs from adopting a misfolded conformation suitable to polymerize into AL fibrils [147]. The inhibitory effect of the  $C_L$  on LC amyloidogenesis led researchers to suggest that the proteolytic cleavage of the monoclonal LC, with the release of the misfolding-prone  $V_L$ , could be the limiting step of the AL fibrils formation.

With this idea in mind and pursuing an explanation to the difference in amyloidogenicity characterizing the LCs, Morgan and Kelly investigated the potential relationship between LC folding stability and susceptibility to proteolysis in a group of AL and non-AL and germline LCs [146]. They found that the intact LCs, even those obtained from AL patients, were unable to form amyloid-like fibrils in physiological conditions. They also found that the folding stability of the LC dimers was kinetically controlled, which agrees with other reports [55,147]. Moreover, they found an inverse correlation between LC kinetic stability and susceptibility to endoproteolysis. LC dimers obtained from AL amyloidosis patients were less kinetically stable and more susceptible to being cleaved into their component domains by proteases, whereas non-amyloidogenic LC dimers were more kinetically stable and resistant to endoproteolysis [146]. Based on these findings, they concluded that, in addition to LC dimer unfolding, endoproteolysis by the appropriate protease, one that affords an amyloidogenic sequence, appears to be required to trigger LC amyloidogenesis [146]. Previous studies have shown that proteolysis of a  $\lambda 6$  rV<sub>L</sub> protein with trypsin [75], as well as Bence Jones proteins with pepsin [148,149] or a preparation of lysosomal proteases [134], generate fragments of the V<sub>L</sub> that form amyloid-like fibrils. Interestingly, Morgan and Kelly did not detect amyloid formation after proteolysis of the LCs with proteinase K, trypsin, or pepsin. Instead, they found that the V<sub>L</sub> of the LCs was rapidly degraded, being released the more stable and non-amyloidogenic C<sub>L</sub>. To overcome this limitation of the experimental model, a thrombin cleavage site was engineered between the two domains of the LC [146]. Although it is a creative solution for probing the concept, such site-directed proteolysis does not reproduce what is expected to occur in tissues well. Therefore, testing the hypothesis that the proteolytic release of amyloidogenic V<sub>L</sub> triggers the formation of AL fibrils in vivo has its main challenge in identifying the acting proteases.

The alternative explanation to LC fragmentation in AL fibrils, that is, that proteolysis occurs after aggregation, has also been investigated. Röcken et al. reported a patient with plasmacytoma of the tonsil with AL amyloidosis caused by a  $\lambda$  LC. They detected two fragments of the LC with different molecular weight but the same N-terminal sequence. This finding and the observation of two different immunostaining patterns of the amyloid deposits in immunogold labeling analysis were interpreted by the authors of this study as evidence of post-fibrillogenetic proteolysis of the fibrillar protein [150]. Enqvist et al. characterized the proteolytic pattern in six patients with AL-amyloidosis of  $\kappa$  type, applying immunotyping with three peptide antisera against two epitopes in the constant segment and one conserved epitope in framework 3 of the V<sub>L</sub>, respectively. They found that the fragmentation pattern was similar in the amyloid of different organs in one patient, but differed greatly between patients. N- and C-terminal fragments and the intact LCs were detected in Western blot analysis with the three antisera. The authors concluded that the results of the study support the hypothesis that the proteolytic cleavage is a post fibrillogenesis event [151]. More recently, Lavatelli et al. applied proteomic analysis for characterizing the fragmentation pattern of AL fibrils extracted from the hearts of two AL cardiomyopathy patients [152]. They found that proteolysis occurs both on the V<sub>L</sub> and C<sub>L</sub> domains, resulting in a complex fragmentation pattern. The structural analysis was consistent with an extensive remodeling of the fibrillar protein by multiple proteases, largely taking place on poorly folded regions of the fibril surfaces. Although not excluding the possibility that the proteolysis of the LC may be a triggering event of AL fibrils formation, the authors concluded that their results indicate that LC deposition largely precedes the proteolytic events documentable in mature AL fibrils [152]. In a very recent publication, the same researchers extended the previous analysis to amyloid deposits obtained from the kidneys and subcutaneous fat of the same patient. It was found that all tissues contain fragments of the LC, along with the intact protein. While the fragment pattern was coincident across organs, microheterogeneity was also detected. Some cleavage positions were the same in all organs, but some were organ specific. Remarkably, it was found that some cleavage sites were not accessible on native dimers, while they are compatible with fibrils. The author concluded that the heterogeneous ensemble of LC fragments originated in tissues,

being consistent with digestion of preformed fibrils, or with the hypothesis that initial proteolytic of the LC triggers AL fibrils formation, followed by subsequent proteolytic degradation [153].

Whether proteolysis occurs before or after LC aggregation is still a matter of debate. However, the available evidence points to the second option as the most likely. Solving this question is critical to understanding the mechanism of in vivo LC amyloidogenesis and may help in identifying factors driving it.

### 3.6. Environmental Factors Modulating the Propensity of LCs to Form Amyloid

The intrinsic propensity of a LC to form amyloid is primarily determined by the amino acid sequence. Hence, much effort has been invested in understanding how the amino acid sequence drives LC aggregation. However, the inability to accurately predict the aggregation behavior of a LC just on the basis of its sequence, and the organ tropism that characterizes the amyloid deposition of these proteins, suggest that factors of the tissue microenvironment can also modulate the aggregation of the LC, influencing both the type and amount of aggregate it forms [60]. Specific components of the extracellular matrix [154], mediators and products of inflammation [155], oxidative stress [131], and receptor-mediated internalization and processing of the LC [156] are factors/mechanisms that have been suggested to promote LC amyloid aggregation. Given their ubiquity in all amyloid deposits, the effects of the extracellular matrix component glycosaminoglycans (GAGs) on LC amyloidogenesis have been investigated by several laboratories. It has been found that the GAG heparan sulfate exerts a differentiated effect on LC aggregation, since it can accelerate the in vitro fibril formation of some LCs, but delays or has no effect on the aggregation of others. In contrast, chondroitin sulfate A predominantly exerts an inhibitory effect on LC aggregation [92,157,158]. Heparan sulfate is believed to accelerate LC fibrillogenesis by promoting the formation of transient amyloidogenic conformations of the protein, whereas the inhibitory effect of chondroitin sulfate A appears to depend on its ability to kinetically trap partially unfolded intermediates, favoring the formation/accumulation of oligomeric/protofibrillar aggregates, but not of fibrils [92]. Taken together, these studies suggest that the effect of GAGs on LC amyloid aggregation depends on both the structural properties of the LC and the GAGs [154]. On the other hand, the interactions between LCs and GAGs may influence the clinical course of disease by enhancing fibril stability and contributing to resistance to protease degradation [154].

A proteomic-based study identified several oxidative post-translational modifications in an amyloidogenic Ig LC from a patient with AL amyloidosis. It was found that some tyrosine residues were heavily mono- or di-chlorinated. Furthermore, a nitrile moiety was observed for many of the terminal aminomethyl groups on lysine side chains [130]. According to a recent study, oxidative post-translational modifications, specifically in tyrosine residues, can promote misfolding and amyloid aggregation of LCs [131]. Inflammatory-derived lipidic aldehydes have also been shown to modulate the in vitro aggregation propensity of the LCs. In vitro studies showed that the aggregation of both  $\kappa$  and  $\lambda$  LCs can be accelerated in the presence of the lipid-derived aldehydes 4-hydroxynonenal, malondialdehyde, glyoxal, atheronal-A, and atheronal-B [155].

Tissues are composed of cells. Consequently, the interaction of amyloidogenic LC with cellular structures, such as the cytoplasmic membrane, can be anticipated to influence LC aggregation [159]. Studies performed in human AC16 cardiomyocytes showed that external amyloid aggregates rapidly surround the cells and act as a recruitment point for soluble protein, triggering the amyloid fibril elongation [160]. However, it has not been determined whether the cytoplasmic membrane can provide a molecular environment in which amyloidogenic LC misfolds and aggregates in vivo. On the other hand, some cell types can internalize the LC by a receptor-mediate mechanism and promote amyloid aggregation intracellularly [156]. This topic is addressed in another section of this review.

#### 4. The Structure of AL Fibrils

The insoluble nature and large molecular size of amyloid fibrils imposed challenging restrictions on any attempt to reveal their internal structure for decades, as they are not suitable for conventional X-ray crystallography or solution NMR analysis, the two most used methods in structural biology. Therefore, several laboratories developed procedures to tailor these methods to the unique properties of amyloid fibrils [161]. Initial clues regarding the internal structure of these aggregates came from X-ray fiber diffraction studies carried out in the 1960s. These studies revealed that amyloid fibrils, irrespective of the constituent protein, yield a common X-ray diffraction pattern known as a cross- $\beta$  pattern. This finding was interpreted in terms of a fibril core formed by a “pleated sheet” structure, with  $\beta$ -strands oriented perpendicular to the fibril axis [162]. Further progress in the elucidation of the amyloid fibril structure required the combination of several biophysical and biochemical techniques [163,164]. As far as we know, the first attempt at modeling the AL fibrils structure was that of Schormann et al., which was based on X-ray crystallography data from the amyloidogenic  $\kappa$ 1 LC BRE [165]. In the early 2000s, studies based on transmission electron and atomic force microscopy allowed a better understanding of the protofilament structure of ex vivo AL fibrils [166] and the assembly mechanism of amyloid-like fibrils [167], respectively. However, it was not until the second half of the 2010s that detailed information on the internal structure of AL fibrils was obtained. This breakthrough was made possible by the implementation of two powerful structural methods suitable for amyloid analysis, solid-state (ss) NMR and cryo-EM [82,85,168,169]. At the time of the completion of this review, six ssNMR-based studies of the LC amyloid fibril structure had been published [87,170–174]. Due to the requirements of this method, the samples analyzed in these studies were synthetic amyloid-like fibrils produced by rV<sub>L</sub> proteins; three of human origin belonging to subgroups  $\kappa$ 1,  $\lambda$ 3, and  $\lambda$ 6, respectively, and one murine. For the purposes of this review, we will focus on two studies, one performed on amyloid-like fibrils of the model protein 6aJL2-R25G [87] and another one performed on amyloid fibrils produced by a  $\lambda$ 3 rV<sub>L</sub> proteins with the sequence of the amyloidogenic LC FOR005 [172]. 6aJL2-R25G protein is a point mutant of the  $\lambda$ 6 germline encoded rV<sub>L</sub> 6aJL2 with Gly replacing Arg25 [87]. Gly25 is an allotypic variant of the V<sub>L</sub> gene segment IGLV6-57 that makes the 6aJL2 protein less thermodynamically stable and more fibrillogenic [83,95]. As mentioned in another part of this review, IGLV6-57 is strongly associated with amyloidosis. The ssNMR analysis showed that the amyloid-like fibrils of 6aJL2-R25G show polymorphism, with three different polymorphs detected in the fibril preparations analyzed. Polymorphs A and B were the most extensively characterized (Figure 4A) [87]. The predicted localization and extent of secondary structural elements in 6aJL2-R25G in the fibrillar state differed substantially from those determined for the native protein by both solution NMR [175] and X-ray crystallography [176] (Figure 4A–C). This led to the conclusion that the assembly of this protein into amyloid-like fibrils occurs through substantial structural conversion that affects the entire molecule [87]. Most assigned residues adopted a  $\beta$ -strand conformation, with the strands being formed both by residues that are situated in  $\beta$ -strands and in former turn regions (Figure 4C). Remarkably, the CDR1 and the loop connecting  $\beta$ -strands E and F (from now on loop E–F), the only two segments of 6aJL2 protein with  $\alpha$ -helix conformation in the native state, also refold into  $\beta$ -strands in the fibrillar protein (Figure 4C). Helix-to-strand transitions have also been found to drive the aggregation of other amyloid precursors, such as prion proteins [177], Apo A–I [178], and A $\beta$  peptides [179,180]. The loop E–F integrated into a long single  $\beta$ -strand that also includes the segments comprising  $\beta$ -strands E and F of the native protein. This structural rearrangement abolishes the loop that forms the CDR3, which illustrates well how extensive the structural adjustments accompanying the fibrillogenesis of 6aJL2-R25G protein are. ssNMR analysis of <sup>15</sup>N:<sup>13</sup>C differentially labeled samples determined that the monomers assemble into fibrils by stacking one on top of the other, in such an ordering that the protein segments in  $\beta$ -strand form parallel in-register intermolecular  $\beta$ -sheets (Figure 4B). The result is several  $\beta$ -sheets running parallel to the fibril axis, which is consistent with the

predictions made based on the XRFD cross- $\beta$  pattern. The spatial arrangement of the monomers and the location and extent of  $\beta$  strands in the molecule support the presence of several pro-amyloidogenic hotspots in the 6aJL2, as was shown in a previous study (Figures 2A and 4A) [75].

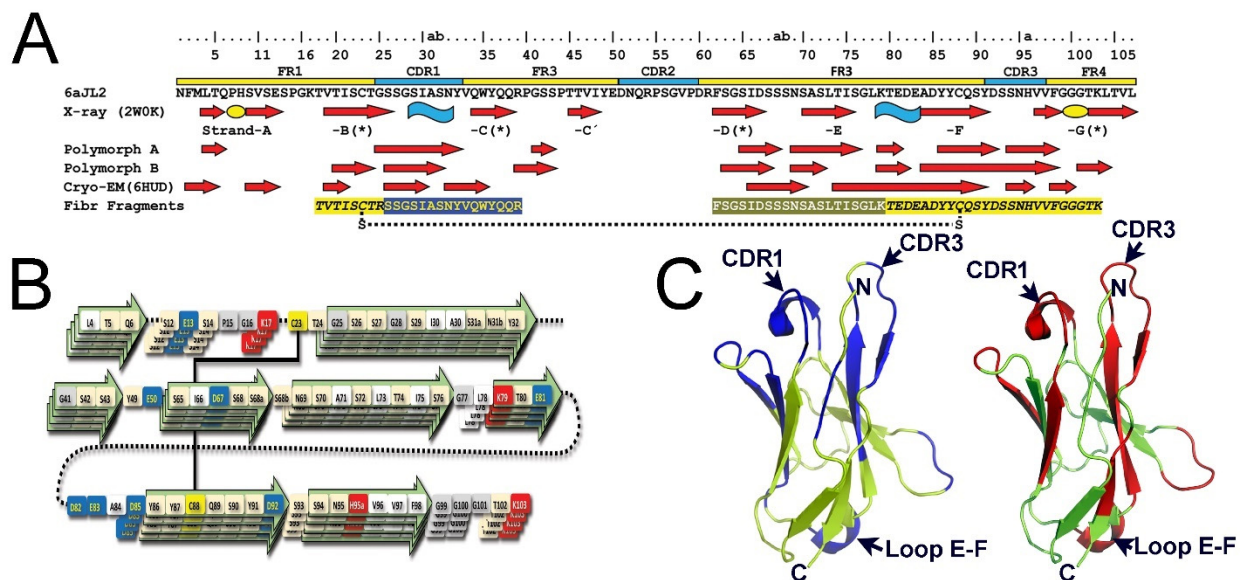


**Figure 4.** ssNMR analysis of the amyloid-like fibrils of the  $\lambda 6$  rV<sub>L</sub> protein 6aJL2-R25G. **(A)** Arrangement of the secondary structure elements of two polymorphs, A and B, of the amyloid-like fibrils formed by the rV<sub>L</sub> protein 6aJL2-R25G, determined by ssNMR analysis [87]. For comparison purposes, the arrangement of secondary structure elements of the native rV<sub>L</sub> protein 6aJL2, determined by X-ray crystallography (PDB 2W0K) [127], and that of the ex vivo AL fibril AL55 ( $\lambda 6$ ), determined by cryo-EM (PDB 6HUD) [85], is shown. The sequence of the three fibrillogenic fragments (Fibr fragments) identified in the protein 6aJL2 using limited proteolysis with trypsin is shown highlighted in colors [75]. The intradomain disulfide bond Cys23-Cys88 that links the two peptide segments composing one of the fibrillogenic fragments is shown as a dotted line.  $\beta$ -strands and  $\alpha$ -helices are represented as red arrows and blue curved ribbons, respectively. The  $\beta$ -strands in the native 6aJL2 protein are indicated according to the standard identification (strand-A to -G). (\*) identified the edge strands of the V<sub>L</sub>  $\beta$ -sandwich. Residue numbering and the complementarity determining (CDRs) and framework (FRs) regions are according to Chothia and Lesk. The yellow ovals in strands A and G represent the structural motifs “sheet-switch” and “ $\beta$ -bulge”. Note that most of the regions of both the rV<sub>L</sub> protein 6aJL2-R25G and the AL LC AL55 that adopt  $\beta$ -strand conformation in their respective fibrillar state overlap with the fibrillogenic fragments of 6aJL2 identified by limited proteolysis. **(B)** Schematic representation of 6aJL2-G25G fibril organization of polymorph A determined by ssNMR analysis. Residues showing in-register parallel orientation are represented by several layers. Protein segments in  $\beta$ -strand are represented as arrows. The intradomain disulfide bond Cys23-Cys88 is displayed as a dotted line. Color code: red and blue denote basic and acid residues, respectively, beige polar non-charged residues, white non-polar residues, yellow cysteine residues, and gray glycine residues. **(C)** Location in the X-ray crystallography structure of 6aJL2 protein (PDB 2W0K) of residues predicted to be in a  $\beta$ -strand in polymorphs A (colored in blue) and B (colored in red). The only two segments of the protein folded in  $\alpha$ -helix, the CDR1 and loop E-F, are indicated.

In another study, Pradhan et al. carried out the ssNMR analysis of synthetic amyloid fibrils of a rV<sub>L</sub> fragment with the sequence of the  $\lambda 3$  AL FOR005 [171,172]. They also characterized fibrils formed by an rV<sub>L</sub> protein with the closest germline sequence of the gene segments encoding FOR005, IGLV3-19 and IGLJ3. This study also included the analysis of point mutants of FOR005, seeking to understand the effect of somatic mutations on the structure of AL fibrils. The analyzed fibrils were produced by seeding the fibrillogenesis of

the isotopically labelled rV<sub>L</sub> protein FOR005 with ex vivo amyloid fibrils purified from the explanted heart of patient FOR005. This procedure aims to propagate the structure of the ex vivo AL fibrils in the isotopically labelled synthetic aggregates, as a way to overcome the inability to analyze natural amyloid with ssNMR. It was found that residues 11–42 and 69–102 adopt  $\beta$ -sheet conformation in the synthetic FOR005 fibrils. The ssNMR data showed that Arg49, a residue introduced in LC FOR005 by somatic mutation, formed a salt bridge with Asp25 in the fibrillar protein. Reverting the mutant Arg49 to the germline encoded Gly in the FOR005 protein caused changes in the fibril's conformation. The point mutation Arg49Gly induced a conformational heterogeneity at the C terminus of FOR005 protein in the fibril's context, whereas the overall fibril topology was retained. Thus, the authors concluded that the saline bridge Arg49-Asp25, generated by a somatic mutation, stabilizes the structure of FOR005 amyloid-like fibrils [172]. It is well-known that somatic mutations can promote the amyloid aggregation of the LCs by destabilizing the LC native folding [88,89]. This study suggests that amyloidogenesis can be promoted by mutations that stabilize the amyloid state, an effect that has been observed in other amyloid precursors [181–183].

It is important to emphasize that the four AL fibrils so far subjected to ssNMR analysis differ from each other in terms of the structure of the fibril's core [87,170–174]. This is primarily a consequence of the high sequence heterogeneity that characterizes light chains.

A fundamental contribution to the elucidation of the structure of AL fibrils has come from the implementation of cryo-EM techniques to the analysis of ex vivo AL fibrils [85,128,168,169]. At the time of completing this review, the structure of four ex vivo AL fibrils, all obtained from patients with cardiac AL amyloidosis, had been deposited in the Protein Data Bank (PDB) (<https://www.rcsb.org/>; data accessed on 2 January 2022). Two structures are of fibrils of  $\lambda$ 1 LCs (PDB 7NSL and 6IC3) [85,128], and the other two are of LCs belonging to subgroups  $\lambda$ 3 (PDB 3Z1O and 3Z1I) [169] and  $\lambda$ 6 (PDB 3HUD) [85], respectively (Figure 5A–D). Cryo-EM analysis showed that the core of the AL fibrils is formed only by the V<sub>L</sub> domain, without involvement of the C<sub>L</sub>. In the fibrils, the V<sub>L</sub> refold into a quasi-bidimensional, flat structure, totally different from the  $\beta$ -sandwich topology characterizing its native state. In all AL fibrils studied so far, the intradomain disulfide bond Cys23-Cys88 is conserved, which indicates that LC misfolding occurs in an oxidative environment [169] (Figure 5A–F). In all fibrils, most of the V<sub>L</sub> segments adopt a defined and stable conformation to form the fibril's  $\beta$ -core, while others, mostly the N- and C-terminals, but also some internal segments, are disordered and exposed to the solvent (Figure 5A–D). A structural motif common to all AL fibrils is the 180° relative rotation, centered on the Cys23-Cys88 disulfide bond, of the segments corresponding to the native  $\beta$  strands B and F. This rearrangement changes the relative orientation N-term to C-term from parallel, characteristic of the native state, to antiparallel [168].

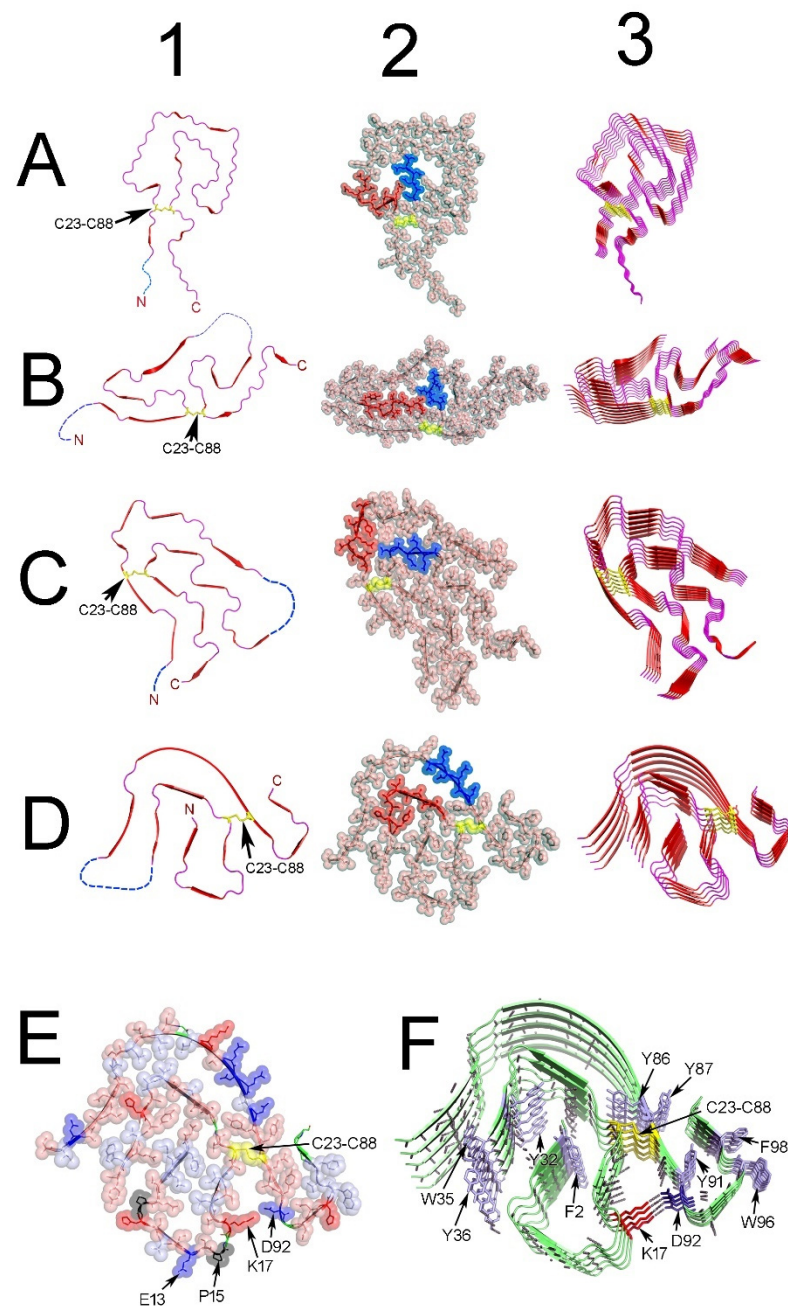


**Figure 5.** Structural models of ex vivo AL fibrils determined by cryo-EM. **(A)** AL fibril formed by a  $\lambda 1$  LC derived from the  $V_L$  gene segment *IGLV1-44*. Structural coordinates contained in the PDB 6IC3 [168]. **(B)** FOR001 AL fibril formed by a  $\lambda 1$  LC derived from the  $V_L$  gene segment *IGLV1-51\*02*. Structural coordinates contained in the PDB 7NSL [128]. **(C)** FOR005 AL fibril formed by a  $\lambda 3$  LC derived from the  $V_L$  gene segment *IGLV3-19\*01*. Structural coordinates contained in the PDB 6Z1O [169]. **(D)** AL fibril formed by the  $\lambda 6$  LC AL55, derived from the  $V_L$  gene segment *IGLV6-57\*02*. Structural coordinates contained in the PDB 6HUD [85]. The four AL fibrils were extracted from cardiac deposits of patients with cardiac AL amyloidosis. Column 1 shows cartoon representations of the  $V_L$  domain polypeptide backbone conformation in the amyloid fibrils. Regions in  $\beta$ -strands are shown with arrows and colored red. Disordered regions are represented as dashed lines in an arbitrary arrangement. Column 2 shows the same structures of column 1, but with the projection of the amino acid side chains, in a combination of semi-transparent spheres/sticks representation, to highlight the side chain-to-side chain interactions that contribute to fibril stability. The amino acid residues spanning the CDR1 and the loop E-F are colored red and blue, respectively. Column 3 shows

the assembly of the AL fibrils by the stacking of the monomers one on the top of another, in register parallel arrangement. In all structures, the conserved intradomain disulfide bond Cys23-Cys88 is represented in a sticks or spheres format and colored yellow. N and C stand for N- and C-terminal. (E,F) show a cartoon representation of the same AL $\lambda$ 6 fibril shown in D, with a detailed representation of the different type of interactions that stabilize the aggregate. In (E), the amino acid side chains are shown in a combined semi-transparent spheres/sticks format, using the following color code: blue for negatively charged (acid) amino acids, red for positively charged (basic) amino acids, salmon for polar non-charged amino acids, light blue for non-polar amino acids, black for proline, and yellow for cysteines. Some residues are indicated for structural reference. Note that non-polar side chains tend to cluster buried in the fibril core, while charged and polar non-charged amino acids tend to locate in the solvent exposed surface. The image in (F) shows the stacking of the monomers of AL55 LC, one on top of the other, in register parallel arrangement. The H bonds between the peptide backbones of adjacent monomers are shown as black dotted lines. Aromatic amino acids interacting by intermolecular stacking are shown. In both images, the conserved intradomain disulfide bond Cys23-Cys88 (colored yellow) and the fibril-specific salt bridge formed by Lys17 and Asp92 is shown. Note that this salt bridge is intermolecular, that is, it is established between residues located in monomers that are contiguous in the fibrillar structure. Regions in  $\beta$ -strands are shown with arrows. Amino acids are identified using a one-letter code. All images were prepared with PyMOL.

Although in all AL fibrils the monomers adopt a flat conformation, the content of  $\beta$  structure and the overall topology of the polypeptide chain differ widely from one fibril to another (Figure 5A–D). Notably, in the  $\lambda$ 6 fibrils, the CDR1 and the N-terminal segment are located in the fibril's inner core [85]. In contrast, in the other ex-vivo AL fibrils, these segments are solvent-exposed at the periphery of the fibril core (Figure 5A–D). It is worth mentioning that the location of the N-terminal segment in the fibril's core in the  $\lambda$ 6 AL fibrils was anticipated in a previous study using single-point mutants to Trp in the N-terminal segment of the germline-encoded rV<sub>L</sub> protein 6aJL2 [94]. Therefore, the possibility cannot be excluded that a buried N-terminal is a shared characteristic of the  $\lambda$ 6 amyloid fibrils, irrespective of whether they are synthetic or natural. Another notable difference between the four ex-vivo AL fibrils is the relative position of the loop E–F. This short segment contains several acid amino acids, and, in the native LCs, it folds in a short  $\alpha$ -helix (Figure 4C). In the structure of the  $\lambda$ 6 AL fibrils, the loop E–F integrates into a long  $\beta$ -strand that form the periphery of the fibril's core, being most of the charged side chain exposed to the solvent. In contrast, this segment is buried in the inner core of the other AL fibrils (Figure 5A–D). The placement of this acidic moiety buried in the fibril's core appears to be partially compensated by a group of charge–charge interactions, and likely by the hydration of the charged side chains by the water molecules filling the internal cavities present in some fibrils (Figure 5A–D) [169].

As predicted by ssNMR studies [87], cryo-EM analysis showed that the AL fibrils form by stacking the V<sub>L</sub> monomers, refolded into a flat conformation, one on top of the other, in a parallel arrangement along the fibril axis [85,168] (Figure 5A–D). By this arrangement, most of the intramolecular contacts that stabilize the tridimensional native folding of the V<sub>L</sub> are substituted by intermolecular contacts between the stacked monomers. The primary force stabilizing the aggregate seems to be the network of H-bonds between the main chain peptide groups of adjacent monomers (Figure 5F). Similar to how fibrillogenic peptides interact with each other in a crystal lattice [76], the amino acid side chains in the AL fibril's core interdigitate each other in a tight complementary fashion, forming steric zipper-like unions (Figure 5A–E). However, in contrast to the self-complementary steric zippers formed by short peptides, in ex vivo AL fibrils, the interactions take place between residues located distantly in the V<sub>L</sub> sequence [86]. Nonpolar amino acids tend to cluster and be buried, while those with polar or charged side chain tend to be solvent-exposed. Aromatic amino acids interact through intermolecular stacking (Figure 5E,F). Remarkably, salt bridges involving residues that do not interact in the native state have been found in all AL fibrils [85,128,168,169] (Figure 5E,F). As mentioned above, fibril-specific salt bridges,

which in some cases result from somatic mutations, can contribute significantly to the stability of the amyloid folding [128,172]. Taken together, cryo-EM data indicate that the AL fibrils are stabilized by a network of polar and non-polar interactions, with important contributions of fibril-specific salt bridges and the highly conserved intradomain disulfide bond Cys23-Cys88.

An interesting characteristic of the ex vivo AL fibrils revealed by cryo-EM is that two conformational forms of the constituent  $V_L$  protein can coexist in the same AL fibril, as was shown in the AL fibril FOR005. This finding implies the occurrence of breaks in the fibrils at the interface of the two conformational forms [169]. Another remarkable contribution of these studies regards the impact of glycosylation, one of the PTM found in the LCs, on the structure of AL fibrils and the aggregation behavior of the soluble precursor [128]. Radamaker et al. determined the cryo-EM structure of the AL fibril FOR001 and found it to be N-glycosylated at Asn18, a residue introduced by somatic mutation [128]. The carbohydrate moiety was located on the surface of the FOR001 fibril, and it was suggested that it could have helped to determine the unique folding of this fibrillar protein [128] (Figure 5B). The effect of the N-glycosylation on the in vitro fibrillogenesis of the LC FOR001 was also evaluated, and it was found to slow down the kinetics of aggregation, which agrees with a previous report [184]. Glycosylation is a PTM frequently found in AL LCs [185,186]. However, the influence of the PTM in the molecular pathogenesis of AL amyloidosis remain poor understood. Radamaker et al. suggested that glycosylation may mask the amyloid deposits within the tissue, preventing their clearance by bodily mechanisms [128]. Using scanning electron microscopy, Radamaker et al. demonstrated that the deposits of AL fibrils infiltrated and disrupted the ordered structure of the cardiomyocytes. They found that the fibrils interacted with the cardiomyocytes surface, mostly through the fibril tips, causing in some cases deformations in the cytoplasmic membrane [128]. Since the fibril deposits compromised the contractile function of the cardiomyocytes, the authors deduced that promoting the remotion of the AL deposits may help to restore the normal cardiac function [128]. Previous studies performed in cell culture demonstrated that soluble LCs obtained from AL patients, but not their non-pathological counterpart, impair the cardiomyocyte contractile function by several mechanisms, including oxidative stress, induction of apoptosis, and inflammatory changes [187–190]. The cytotoxic effect of synthetic AL fibrils on cultured cardiomyocytes has also been studied [160]. However, as far as we know, the study conducted by Radamaker et al. is the first to provide structural evidence of one mechanism by which AL fibrils interfere the contractile function of cardiomyocytes at organ level [128].

Some conclusions that arise from the cryo-EM studies are as follows: (1) LC amyloid aggregation implies the extensive structural conversion of the  $V_L$  into a quasi-bidimensional structure, (2) the AL fibril core is formed by several segments of the  $V_L$ , some of them folded in loops and turns and other in  $\beta$ -strand that associate in long intermolecular  $\beta$ -sheets, and (3) the topology adopted by the  $V_L$  in AL fibrils differs from one AL aggregate to another and appears to be mainly determined by protein-dependent factors, such as the primary structure and PTMs. However, environmental factors, such as the composition of the extracellular matrix [191] and the interaction with the amyloid accessory molecules [192], could also exert an important influence.

The comparison of the data generated by ssNMR [172] analysis of the synthetic amyloid-like fibrils FOR005 with those obtained by cryo-EM [169] in ex vivo AL fibrils FOR005 demonstrated that there are structural differences between these two types of aggregates. This is a remarkable finding, considering that the preparation of synthetic amyloid-like fibrils was produced by seeding the recombinant  $rV_L$  protein FOR005 with ex vivo FOR005 fibrils. Such differences likely are the consequence of the different environmental conditions in which these aggregates were generated, as well as the influence of factors that have been shown to modulate the aggregation propensity of the amyloidogenic LCs. Some of these factors are the components of the extracellular matrix and the molecules that are closely associated with the fibrillar component in all amyloid deposits, known

as accessory components of the amyloid [192]. The possibility cannot be excluded that variables, such as the age of the aggregates, and the conformational restriction that the  $C_L$  could have imposed the *in vivo* assembly of FOR005 LC into fibrils, but that was absent in the seeding of the  $rV_L$  protein FOR005, could explain part of the observed differences. The  $rV_L$  proteins were for a long time the preferred model to study the mechanism of formation and the structure of LC amyloid fibrils, and they are still a frequently used models in this field. Determining the origin and extending the observed structural differences between synthetic and *ex vivo* AL fibrils will help in establishing the uses and limitations of the  $rV_L$  proteins as research model.

Despite the aforementioned discrepancies, the studies based on both ssNMR and Cryo-EM analysis have confirmed that structural heterogeneity is the hallmark of the AL fibrils. The monoclonal LC that causes AL deposition is unique for each patient, as is the internal structure and pathological properties of the fibrillar and non-fibrillar aggregates that it produces. All this, in interplay with the unique genetic background and biological momentum of the affected individual, results in a disease that, although named for practical purpose “AL amyloidosis”, is actually a patient-specific disorder [54]. This concept must be considered by both physicians and researchers dealing with this disease.

### 5. Mechanism of Misfolding and Assembly of the LC into Amyloid Fibrils

Misfolding is key in LC amyloid aggregation. ssNMR and cryo-EM data support a model of AL fibrils assembly in which the amyloid conformation of the LC is reached through the total unfolding of the protein [85,87,168,169,171,172]. However, how this unfolding-refolding mechanism occurs has not been clarified yet. A central issue in this regard is the structural characteristics of the molecular species that drive aggregation. This question is relevant not only to understanding the mechanism of AL fibril formation but also to identify the most suitable target(s) for therapies aimed at inhibiting LC amyloidogenesis. It is worth mentioning that, as with most amyloid precursors, LCs form amyloid *in vitro* with nucleation-dependent kinetics, characterized by a lag phase followed by a logarithmic growth phase [102]. Several studies carried out with  $rV_L$  proteins found a positive correlation between the duration of the latency phase and the folding stability of the protein [83,88,90,91,94–96,100–102,193,194]. Therefore, it was deduced that some degree of alteration of the native folding of the fibril precursor is required for it to nucleate fibrillogenesis. The evidence suggests that non-native partially unfolded intermediates, but not the fully unfolded conformers, are the species that most efficiently promote fibrillogenesis [97,101,104,144]. Fink’s laboratory studied the effect of both low pH [144] and concentration of guanidine hydrochloride, a chaotropic denaturant, on the fibrillogenesis of the amyloidogenic  $\kappa 4$   $rV_L$  protein SMA. In both conditions, two different partially folded intermediates were detected, one native-like, which predominantly formed amorphous deposits, and a more unfolded intermediate that formed fibrils more rapidly [104,144]. They also obtained evidence indicating that fibril elongation involved the addition of a partially unfolded intermediate, rather than the native state [104]. Therefore, it was concluded that a more highly unfolded intermediate is more suited to undergo the topological rearrangements necessary to form amyloid fibrils than a more structured one [104].

Blancas-Mejia et al. also found evidence of a partially folded intermediate in the fibrillogenesis pathway of the  $\lambda 6$   $rV_L$  protein 6aJL2 [101]. Using urea as a destabilizing agent, a partially unfolded off-pathway intermediate around the midpoint of the urea unfolding curve of the protein was detected [101]. The maximum growth rate for fibril formation and the minimum lag time were measured at urea concentrations where the partially unfolded intermediate was populated, suggesting its involvement in the aggregation pathway [101]. Biophysical data indicated that the amyloidogenic intermediate was a soluble oligomeric state [101]. Overall, the aforementioned studies support the notion that the conformational species of the  $rV_L$  proteins that most efficiently promote fibrillogenesis are partially unfolded intermediates characterized by a substantial loss of

native folding. Persistence of some secondary and tertiary structure seems to be necessary for fibrillogenesis to occur [195].

It is important to mention that, for the sake of experimental efficiency, most of the above-cited studies used destabilizing, non-physiological conditions of pH or denaturant concentration, aimed at increasing the probability of detecting non-native intermediates of the experimental protein. However, some rV<sub>L</sub> proteins efficiently form amyloid-like fibrils under physiological conditions of pH, ionic strength, and temperature, where the protein unfolded fraction is very small [83,94,95,107,193]. Therefore, it cannot be excluded that, under physiological conditions, the fibrillogenesis of at least some rV<sub>L</sub> proteins occurs through complex pathways involving different conformational species, including native-like folding intermediates. In a recent report, Kazman et al. dissected the lag phase of the *in vitro* fibrillogenesis of a patient-derived V<sub>L</sub> protein and characterized the structural transitions that preceded fibril formation [196]. It was found that the aggregation started with partial unfolding of the V<sub>L</sub> domain and the formation of small amounts of dimers, which was followed by the formation of an ensemble of oligomers. Remarkably, they found that oligomerization was accompanied by structural adjustment of the hydrophobic core of the V<sub>L</sub> protein, which included changes in solvent accessibility and rigidity and structural transitions from an anti-parallel to a parallel  $\beta$ -sheet secondary structure. All these structural changes, which are consistent with a global conformational transition of the V<sub>L</sub>, took place in the oligomers prior to amyloid formation [196]. Moreover, it was found that the formation of a non-native dimer was a prerequisite for the formation of the ensemble of oligomers, the context where the most extensive structural rearrangement of the V<sub>L</sub> domain took place [196]. It is worth mentioning that some rV<sub>L</sub> proteins form stable dimers that protect them from aggregation. The evidence indicates that a limiting step for the fibrillogenesis of these proteins is the dissociation of the native dimer into misfolded-prone monomers [132,135,197–199]. Therefore, it cannot be excluded that some rV<sub>L</sub> proteins form fibrils through a pathway that starts on a native dimer, which dissociate into misfolded-prone monomers, which subsequently reassociate into non-native dimers.

Previous studies have shown that amyloidogenic LCs, but not their non-pathological counterpart, tend to form high molecular weight aggregates under physiological conditions [200]. Hence, it is important to establish whether the mechanism of fibrillogenesis revealed by Kazman et al. is characteristic of V<sub>L</sub>s derived from amyloidogenic LCs, or an attribute common to all V<sub>L</sub>s. Moreover, it is also important to establish whether this mechanism applies to full-length LCs, in view of the known influence of the C<sub>L</sub> domain on the aggregation properties of the full-length LC [55,145].

## 6. Role of the Mesangial Cells in Glomerular Amyloidosis: Are They an Amyloid Factory?

Conceptually, amyloid aggregation is described as a pathological event driven by protein misfolding [201,202]. Therefore, much research in this field has focused on the *in vitro* characterization of the amyloid precursors, seeking to identify the structural and biophysical properties that make them prone to aggregation. This approach has allowed a better understanding of the mechanistic aspects of amyloidogenesis from a protein perspective, being also valuable for the screening of inhibitors of amyloidogenesis [103,148,149,203–209]. Amyloid fibrils can be produced in cell-free systems, but this represents a situation far distant from reality in humans where the circulating amyloid precursors must interact with tissue elements in the formation of amyloid fibrils. Amyloid aggregation occurs mostly in the extracellular compartment, in the presence of molecules with very diverse structural properties and activity. This includes proteases and other proteins with very diverse functions, such as transporters, receptors, ion channels, and structural proteins, as well as lipids, glycoconjugates, and ions, among others. These compounds assemble into complex biological structures, such as the cytoplasmic membrane and the extracellular matrix, with which the amyloid precursor interacts, with its aggregation behavior being modulated by this molecular microenvironment [210,211].

Moreover, the accumulation of the amyloid aggregates and other non-native species of the precursor leads to the activation of biological processes that end up with cell damage, phenotype transformation, and extracellular matrix remodeling, common events in the pathogenesis of amyloidosis [212–215]. Therefore, the accurate understanding of amyloidogenesis, as a pathological phenomenon, requires revealing the complex interplay between the amyloid precursor and the numerous components of the microenvironment where aggregation takes place.

For more than three decades, the role of cells in participating in the process of amyloidogenesis has been explored by a number of investigators. There are abundant publications addressing the contributions of cells to the A $\beta$  precursor protein processing and aggregation [216–218]. The important role that macrophages play in amyloidogenesis, particularly in serum amyloid A protein-derived (AA) amyloidosis, has also been investigated with some rigor [219–222]. However, the role of mesangial cells in the AL deposition in the renal glomerulus, as well as pericytes/smooth muscle cells in the vasculature, has been advanced considerably in recent years, as they participate in LC-associated amyloidosis [59,156,214]. In this part of the review, we focus on mesangial cells as facilitators of LC amyloidogenesis in the renal glomerulus and mediators of pathological remodeling of the mesangium, but also as targets for the harmful activity of amyloidogenic LC and its aggregates.

The monoclonal LC interaction with different cell types has been shown to depend on the ability of certain cells to internalize this amyloid precursor and manufacture the fibrils in the mature lysosomal compartment, which is related to the physicochemical characteristics of the particular precursor proteins [223–225]. Signaling mechanisms involved in the process are crucial to understand how amyloid fibril formation occurs and to eventually develop pharmacologic maneuvers to stop or ameliorate this process once the inciting pathological activity has been controlled or curtailed.

The kidney receives approximately 25% of the cardiac output and any circulating proteins will be delivered to the kidneys where interaction with renal cells must occur. Monoclonal LCs circulate in patients with plasma cell dyscrasias and, because of their low molecular weight, they are normally filtered through the capillary walls and delivered to the proximal tubules where normal LCs are internalized using the cubilin/megalyn receptor and metabolized by lysosomes returning the amino acids to the circulation [226,227].

Some of these monoclonal LCs are attracted to the glomerulus, more specifically the mesangium, where pathological changes occur. The interaction of these glomerulopathic LCs with mesangial cells involve a receptor: SORL1 [156]. It is important to highlight that the final pathologic changes that occur in the glomeruli depend on the glomerulopathic LCs involved and the alterations in the mesangium are regulated by the surface activities that take place between involving mesangial cells [228–230]. The same is true about the vasculature where these circulating monoclonal LCs interact with pericytes/smooth muscle cells to produce amyloid [214]. The processes that take place in the renal mesangium and in the vasculature in AL-amyloidosis are amazingly similar.

The signaling mechanisms that must occur for the cells to become primed for amyloidogenesis have also been dissected [223,231,232]. Two factors control the mesangial cell activities leading to AL fibrils formation. C-fos and NF- $\kappa$ B are instrumental in fostering cellular activities that control amyloidogenesis. C-fos is necessary for phenotypic transformation of mesangial cells into a macrophage phenotype [223,232], a crucial event that needs to occur before mesangial cells can engage in active amyloid formation. Signals are activated when glomerulopathic LCs interact with mesangial cells at the cell surfaces and become endocytosed, an event that is instrumental in leading the internalized LCs into the mature lysosomal system for processing (Figure 6A–C). Once in the lysosomes, helped by the stringent low pH and the likely presence of protease, processing of the LC is carried out and formation of fibrils occurs [233] (Figure 6D). The last step involves the exocytosis of the fibrils into the extracellular compartment [230] (Figure 7A–F). Once in the extracellular compartment, there is activation of metalloproteinases and replacement of the mesangial matrix with AL fibrils (Figure 6D). Amyloid also inhibits TGF- $\beta$  significantly,

compromising the repair of the altered extracellular matrix. LCs also potentiate apoptosis of mesangial cells. The combination of these effects leads to the expansion of mesangial areas with the deposition of AL fibrils and the replacement of the mesangial matrix, as well as the disappearance of the mesangial cells resulting in the appearance of acellular mesangial nodules in the end-stage of this disease process [229]. Once extracellular amyloid is present, additional amyloidogenesis occurs exponentially by progressive extension of this process after the initial seeding has taken place (Figure 6D). A similar mechanism has been proposed for extracellular amyloid plaque formation during Alzheimer's disease pathogenesis [234]. Cell-dependent seeding may function as the triggering mechanism for LC amyloid deposition at the tissue scale. Alternatively, it may operate in parallel with other cell-independent mechanisms of LC amyloidogenesis, contributing to the amyloid burden of the organ. More research is required to establish the potential contribution of mesangial cells, as well as other cells with the capacity to internalize amyloidogenic LCs, in the initiation and dissemination of AL deposits.

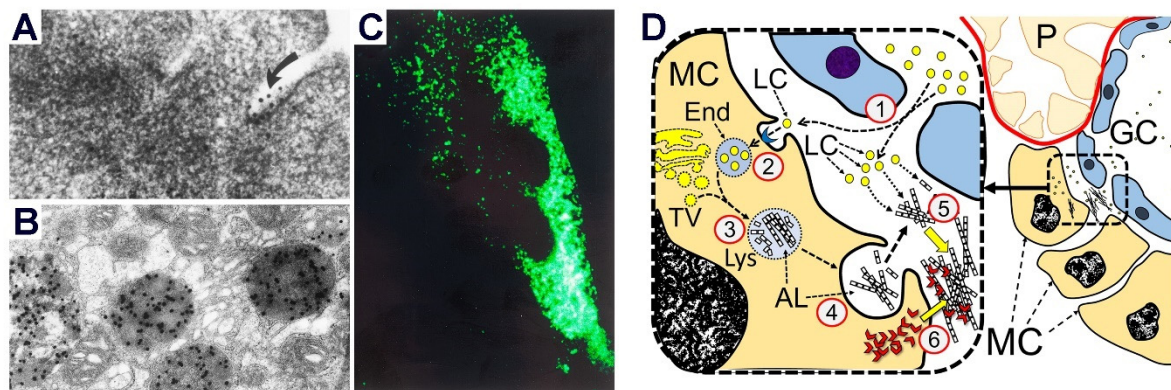


**Figure 6.** Experimental demonstration and schematic representation of the multistep process of AL LC internalization and processing in MCs. (A,B) Immunogold labeling (10 nm gold particles) transmission electron microscopy, with uranyl acetate and lead citrate staining, in MCs incubated with AL LCs purified from urine of a patient with renal AL-amyloidosis. In (A), note an early interaction of light chains (labeled with gold particles) with surface caveola in mesangial cell (A) after 4–6 h of incubation. In (B), note the same LCs within lysosomes 24 h after incubation. (C) Direct immunofluorescence detection (fluorescein isothiocyanate) of internalized AL LCs in mesangial cells incubated with AL LCs, as described in (A). Note the presence of fluorescence in the cytoplasmic space, indicative of internalization of AL LC in the mesangial cell. Augmentations: A  $\times 35,000$ ; B  $\times 32,500$ ; C  $\times 500$ . (D) Diagrammatic representation of AL LC internalization and processing in MCs. (1) The unstable and misfolding-prone monoclonal LC (yellow circles) is filtered from the glomerular capillary (GC). (2) The LC internalizes into the MCs by a receptor-mediated mechanism. (3) The late endosomes (End) containing the misfolded LC fuse with transport vesicles carrying lysosomal hydrolases and transform into lysosomes (Lys), where the acidic pH and likely the proteolysis by lysosomal proteases promote the self-assembly of the LC into amyloid fibrils. (4) The AL fibrils formed inside the lysosomes are extruded from the MC, accumulating in the extracellular space. (5) The extruded amyloid fibrils seed the fibrillogenesis of soluble LC monomers. Fibrils accumulate in the extracellular space. (6) MMPs and other proteases secreted by the MCs proteolyze the AL fibrils, removing the protease-sensitive  $C_L$  domain of the aggregated LC, as well as other components of the extracellular matrix. This results in substitution of the extracellular matrix by AL fibrils. Experimental data support steps 1–4. In steps 5 and 6, a possible mechanism of AL amyloid deposition in the glomeruli mediated by mesangial cells (MCs) is proposed. P stands for podocyte.

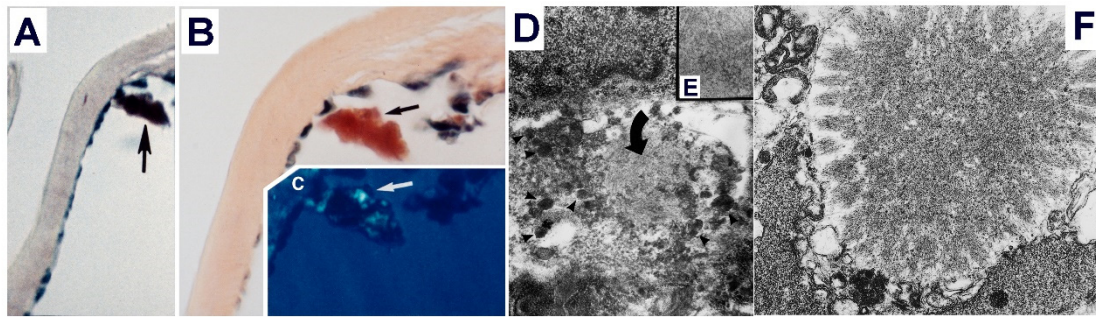


**Figure 7.** Manufacturing of AL fibrils by the mesangial cells. (A–C) Mesangial cells growing on Matrigel incubated with AL-LCs for 48 h. (A) Hematoxylin and eosin; (B) Congo red; and (C) polarization of Congo red stained section. Note in A the eosinophilic amorphous material (amyloid) produced by mesangial cells. This material is Congo red-positive (B) and apple green birefringent when polarized (C). Augmentations: A  $\times 200$ ; B  $\times 400$ ; C  $\times 200$ . (D,E) Mesangial cells incubated with AL-LCs for 72 h. Transmission electron microscopy; uranyl acetate and lead acetate. Note in D amyloid fibrils (arrow) manufactured by surrounding mesangial cells with macrophage phenotype. Note in E numerous lysosomes in the cytoplasm of mesangial cells and loss of myofilaments. Augmentations: D  $\times 22,500$ ; E  $\times 35,000$ . (F) Mesangial cells incubated with AL-LCs for 96 h. Note the cumulation of extracellular amyloid fibrils and lysosomes abutting cell membranes of mesangial cells and gaps in the cell membranes permitting exiting of amyloid fibrils. Augmentations:  $\times 30,500$ .

The presence of cells capable of endocytosing the amyloid precursor appears to be a crucial element for amyloidogenesis to occur in at least the most common types of amyloidosis: AA and AL amyloidosis [221,222]. Patients with disseminated amyloidosis almost invariably have involved organs and sites rich in macrophages or with resident cells that have the ability to phenotypically transform into cells with abundant lysosomes (so-called “macrophage phenotypic transformation”) (Figure 8A–G). The systemic vascular deposition of fibrils in systemic amyloidosis represents further evidence of the role of cellular transformation permitting lysosomal processing of internalized amyloid precursors into fibrils.

Without the cellular component, what happens in glomeruli engaged in amyloidosis would not occur. The mesangial cells are intimately involved, playing a crucial role in glomerular amyloidogenesis to a point where they are an essential element in this process. As animal models of amyloidogenesis are developed, issues of pathogenetic interest such as LC tropism and genetic modifiers become very important; these require further studies. It should be emphasized that only models with cellular components are capable of reproducing what occurs in humans and create testing grounds for realistic development of new therapeutic interventions. In vitro models lack the cellular element that is so fundamental in human disease (amyloidosis).

In the last 3 decades, notable experimental developments have taken place that create the perfect environment for the development of novel therapeutic interventions. One crucial development has been that of stem cell therapy as a mechanism to replace the damaged mesangium in glomeruli and repair overall renal parenchyma [235–238]. While this is still in its early phases, much hope remains. Some of the platforms used to study the ability of mesenchymal stem cells in repair mimic quite closely the glomerular alterations that are seen in renal biopsies from patients with glomerular AL amyloidosis facilitating translational studies. Combining these with the information that has been gained from in vitro research in amyloidosis provides a perfect set-up for extending studies aiming at repairing the tissue damage caused by amyloid deposition. The concept that amyloid fibrils are tombstones is no longer tenable, as the fibrillary material and oligo amyloid components are involved in direct tissue damage, as has been demonstrated in the laboratory and confirmed clinically in biopsy material [239].

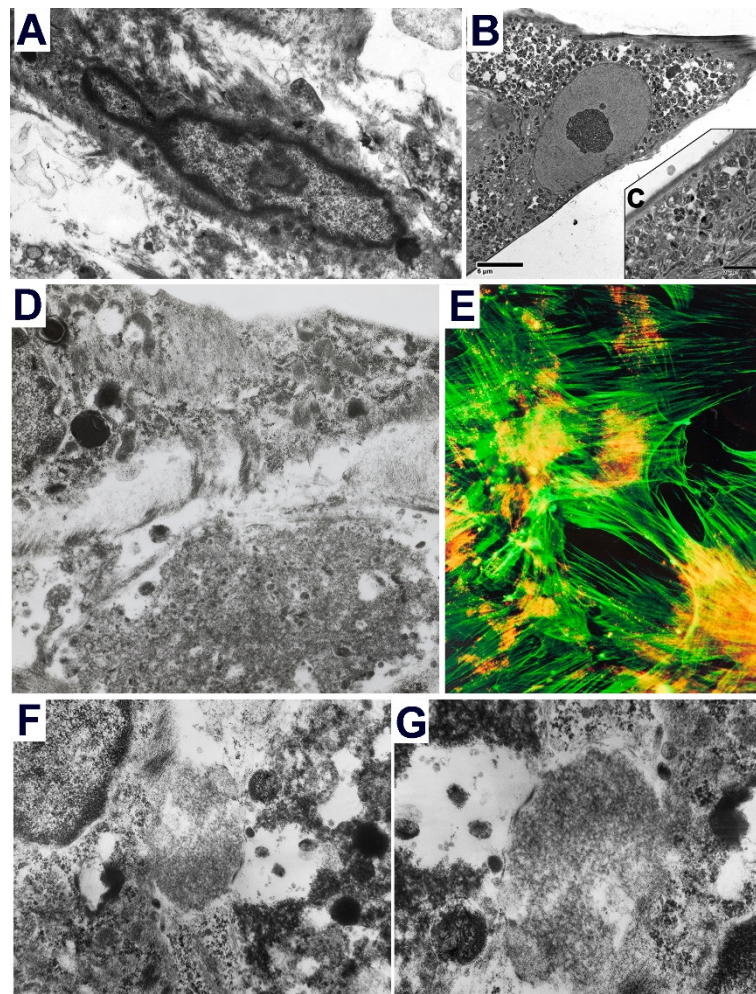


**Figure 8.** Interaction of mesangial cells with AL LCs results in phenotype transformation. (A–C) Transmission electron microscopy with uranyl acetate and lead acetate staining of mesangial cells culture on a matrix (Matrigel) and incubated with AL-LCs for 24 h. Note in A the typical ultrastructure of mesangial cells with intracellular myofilament bundles and lack of lysosomes. Note in B that mesangial cell has lost its cytoplasmic filaments, except focally. (C) (insert) Note that the mesangial cell cytoplasm is filled with variably sized lysosomes (C). Augmentations: A  $\times 950$ ; B  $\times 800$ ; C  $\times 6000$ . (D) Transmission electron microscopy with uranyl acetate and lead citrate staining of mesangial cells incubated with AL-LC. Note mesangial cells with macrophage phenotype engaged in manufacturing of amyloid fibrils. Augmentations:  $\times 12,500$ . (E) F-actin detected by fluorescein isothiocyanate fluorescence staining in mesangial cells incubated with AL LCs. Double staining with Texas red labeled CD68. Note hybrid mesangial cells exhibiting typical actin cytoarchitecture and CD68 expression with colocalization (yellow staining areas). (F,G) Transmission electron microscopy with uranyl acetate and lead acetate staining of MCs incubated with AL LCs for 48 h. Note the extracellular amyloid fibrils produced by adjacent MCs with a macrophage phenotype (with multiple intracytoplasmic lysosomes and loss of microfilaments) Augmentations: F  $\times 38,500$ ; G  $\times 23,500$ .

## 7. Challenges in AL Amyloidosis Research

The AL amyloidosis is unique among all amyloidoses due to the unparalleled sequence diversity of the involved precursor, the immunoglobulin LCs [54]. Such a characteristic makes it exponentially more complicated to understand the structural bases and pathophysiology of the disease. Recent cryo-EM-based studies have shown that, structurally, AL fibrils are comparatively much more heterogeneous than any other type of amyloid [85,128,168,169]. Basically, the conformation of the LC in the AL fibrils deposited in each AL patient is unique, a characteristic that, as it interplays with the biological sin-

gularity of the affected individual, results in a patient-specific disease [240,241]. Thus, the structural heterogeneity of the LCs establishes several challenges to AL amyloidosis research. One of the most relevant is to understand how the interplay between the structural and biophysical properties of the monoclonal LC and factors of the tissue microenvironment determines three key aspects of AL amyloidosis: (1) the pathogenic properties of the circulating misfolding-prone LC, (2) the organ tropism of LC amyloid deposition, and (3) the structure and pathogenic properties of AL fibrils. To the extent that it is possible to overcome these challenges, opportunities will be created for the development of new therapeutic strategies that interrupt the complex chain of pathogenic events that begin with the LC misfolding, involves its aggregation into AL fibrils and other structurally diverse non-native species, and ends with irreversible organ damage.

## 8. Conclusions

The last decade has seen significant progress in our understanding of the mechanism of amyloid aggregation of the LCs and, above all, of the structure of AL fibrils. The presence of several pro-amyloidogenic hotspots scattered throughout the  $V_L$  of LCs has been demonstrated. The data indicate that these regions participate in the AL fibril assembly mechanism, which requires extensive structural conversion of the domain to a quasi-bidimensional entity. Although this step is common to the amyloid aggregation of all LCs, the conformation of the  $V_L$  in the fibrillar state differs widely between AL fibrils derived from different LCs. Such structural heterogeneity of the AL fibrils, which is primarily a reflection of the structural diversity of LCs, also appears to depend on other factors, such as post-translational modifications of the precursor, and proteolysis of the aggregate. To all of the above, we must add the role of cells in the pathogenesis of the disease, both as the target of the harmful properties of the amyloidogenic LC and its aggregated forms, as well as a potential factory of AL amyloid, causing the dissemination of deposits.

**Author Contributions:** Conceptualization, L.D.P.-Y. and G.A.H.; writing—original draft preparation, L.D.P.-Y., G.A.H., J.I.P.-C. and E.A.T.-H., writing—review and editing, L.D.P.-Y., G.A.H., J.I.P.-C. and E.A.T.-H. All authors have read and agreed to the published version of the manuscript.

**Funding:** This research received no external funding. APC was sponsored by MDPI.

**Institutional Review Board Statement:** Not applicable.

**Informed Consent Statement:** Not applicable.

**Acknowledgments:** We thank Adrian Hoff for his valuable contribution in the preparation of figures.

**Conflicts of Interest:** All the authors declared no competing interests.

## References

1. Vogel, C.; Bashton, M.; Kerrison, N.D.; Chothia, C.; Teichmann, S.A. Structure, function and evolution of multidomain proteins. *Curr. Opin. Struct. Biol.* **2004**, *14*, 208–216. [[CrossRef](#)] [[PubMed](#)]
2. Shin, D.H.; Hou, J.; Chandonia, J.M.; Das, D.; Choi, I.G.; Kim, R.; Kim, S.H. Structure-based inference of molecular functions of proteins of unknown function from Berkeley Structural Genomics Center. *J. Struct. Funct. Genom.* **2007**, *8*, 99–105. [[CrossRef](#)] [[PubMed](#)]
3. Nassar, R.; Dignon, G.L.; Razban, R.M.; Dill, K.A. The Protein Folding Problem: The Role of Theory. *J. Mol. Biol.* **2021**, *433*, 167126. [[CrossRef](#)]
4. Dunker, A.K.; Obradovic, Z.; Romero, P.; Garner, E.C.; Brown, C.J. Intrinsic protein disorder in complete genomes. *Genome Inf. Ser. Workshop Genome Inf.* **2000**, *11*, 161–171.
5. Malagrino, F.; Diop, A.; Pagano, L.; Nardella, C.; Toto, A.; Gianni, S. Unveiling induced folding of intrinsically disordered proteins - Protein engineering, frustration and emerging themes. *Curr. Opin. Struct. Biol.* **2021**, *72*, 153–160. [[CrossRef](#)] [[PubMed](#)]
6. Gonzalez-Perez, P.P.; Orta, D.J.; Pena, I.; Flores, E.C.; Ramirez, J.U.; Beltran, H.I.; Alas, S.J. A Computational Approach to Studying Protein Folding Problems Considering the Crucial Role of the Intracellular Environment. *J. Comput. Biol.* **2017**, *24*, 995–1013. [[CrossRef](#)] [[PubMed](#)]
7. Stefani, M.; Dobson, C.M. Protein aggregation and aggregate toxicity: New insights into protein folding, misfolding diseases and biological evolution. *J. Mol. Med.* **2003**, *81*, 678–699. [[CrossRef](#)]

8. Peng, P.H.; Hsu, K.W.; Wu, K.J. Liquid-liquid phase separation (LLPS) in cellular physiology and tumor biology. *Am. J. Cancer Res.* **2021**, *11*, 3766–3776.
9. Lu, J.; Qian, J.; Xu, Z.; Yin, S.; Zhou, L.; Zheng, S.; Zhang, W. Emerging Roles of Liquid-Liquid Phase Separation in Cancer: From Protein Aggregation to Immune-Associated Signaling. *Front. Cell Dev. Biol.* **2021**, *9*, 631486. [[CrossRef](#)]
10. Carey, J.L.; Guo, L. Liquid-Liquid Phase Separation of TDP-43 and FUS in Physiology and Pathology of Neurodegenerative Diseases. *Front. Mol. Biosci.* **2022**, *9*, 826719. [[CrossRef](#)]
11. Temussi, P.A.; Tartaglia, G.G.; Pastore, A. The seesaw between normal function and protein aggregation: How functional interactions may increase protein solubility. *Bioessays* **2021**, *43*, e2100031. [[CrossRef](#)] [[PubMed](#)]
12. Yang, H.; Li, J.J.; Liu, S.; Zhao, J.; Jiang, Y.J.; Song, A.X.; Hu, H.Y. Aggregation of polyglutamine-expanded ataxin-3 sequesters its specific interacting partners into inclusions: Implication in a loss-of-function pathology. *Sci. Rep.* **2014**, *4*, 6410. [[CrossRef](#)] [[PubMed](#)]
13. Bucciantini, M.; Calloni, G.; Chiti, F.; Formigli, L.; Nosi, D.; Dobson, C.M.; Stefani, M. Prefibrillar amyloid protein aggregates share common features of cytotoxicity. *J. Biol. Chem.* **2004**, *279*, 31374–31382. [[CrossRef](#)] [[PubMed](#)]
14. Limbocker, R.; Mannini, B.; Ruggeri, F.S.; Cascella, R.; Xu, C.K.; Perni, M.; Chia, S.; Chen, S.W.; Habchi, J.; Bigi, A.; et al. Trodusquemine displaces protein misfolded oligomers from cell membranes and abrogates their cytotoxicity through a generic mechanism. *Commun. Biol.* **2020**, *3*, 435. [[CrossRef](#)]
15. Stefani, M. Biochemical and biophysical features of both oligomer/fibril and cell membrane in amyloid cytotoxicity. *FEBS J.* **2010**, *277*, 4602–4613. [[CrossRef](#)]
16. Bemporad, F.; Ramazzotti, M. From the Evolution of Protein Sequences Able to Resist Self-Assembly to the Prediction of Aggregation Propensity. *Int. Rev. Cell Mol. Biol.* **2017**, *329*, 1–47. [[CrossRef](#)] [[PubMed](#)]
17. Monsellier, E.; Chiti, F. Prevention of amyloid-like aggregation as a driving force of protein evolution. *EMBO Rep.* **2007**, *8*, 737–742. [[CrossRef](#)]
18. Begum, T.; Ghosh, T.C. Understanding the effect of secondary structures and aggregation on human protein folding class evolution. *J. Mol. Evol.* **2010**, *71*, 60–69. [[CrossRef](#)]
19. Das, M.; Gursky, O. Amyloid-Forming Properties of Human Apolipoproteins: Sequence Analyses and Structural Insights. *Adv. Exp. Med. Biol.* **2015**, *855*, 175–211. [[CrossRef](#)]
20. Sant'Anna, R.; Braga, C.; Varejao, N.; Pimenta, K.M.; Grana-Montes, R.; Alves, A.; Cortines, J.; Cordeiro, Y.; Ventura, S.; Foguel, D. The importance of a gatekeeper residue on the aggregation of transthyretin: Implications for transthyretin-related amyloidoses. *J. Biol. Chem.* **2014**, *289*, 28324–28337. [[CrossRef](#)]
21. De Baets, G.; Van Durme, J.; Rousseau, F.; Schymkowitz, J. A genome-wide sequence-structure analysis suggests aggregation gatekeepers constitute an evolutionary constrained functional class. *J. Mol. Biol.* **2014**, *426*, 2405–2412. [[CrossRef](#)] [[PubMed](#)]
22. Richardson, J.S.; Richardson, D.C. Natural beta-sheet proteins use negative design to avoid edge-to-edge aggregation. *Proc. Natl. Acad. Sci. USA* **2002**, *99*, 2754–2759. [[CrossRef](#)] [[PubMed](#)]
23. Foy, S.G.; Wilson, B.A.; Bertram, J.; Cordes, M.H.J.; Masel, J. A Shift in Aggregation Avoidance Strategy Marks a Long-Term Direction to Protein Evolution. *Genetics* **2019**, *211*, 1345–1355. [[CrossRef](#)] [[PubMed](#)]
24. Esperante, S.A.; Varejao, N.; Pinheiro, F.; Sant'Anna, R.; Luque-Ortega, J.R.; Alfonso, C.; Sora, V.; Papaleo, E.; Rivas, G.; Reverter, D.; et al. Disease-associated mutations impacting BC-loop flexibility trigger long-range transthyretin tetramer destabilization and aggregation. *J. Biol. Chem.* **2021**, *297*, 101039. [[CrossRef](#)] [[PubMed](#)]
25. Bartels, T.; Choi, J.G.; Selkoe, D.J. alpha-Synuclein occurs physiologically as a helically folded tetramer that resists aggregation. *Nature* **2011**, *477*, 107–110. [[CrossRef](#)]
26. Hammarstrom, P.; Jiang, X.; Hurshman, A.R.; Powers, E.T.; Kelly, J.W. Sequence-dependent denaturation energetics: A major determinant in amyloid disease diversity. *Proc. Natl. Acad. Sci. USA* **2002**, *99* (Suppl. S4), 16427–16432. [[CrossRef](#)]
27. Wyatt, A.; Yerbury, J.; Poon, S.; Dabbs, R.; Wilson, M. Chapter 6: The chaperone action of Clusterin and its putative role in quality control of extracellular protein folding. *Adv. Cancer Res.* **2009**, *104*, 89–114. [[CrossRef](#)]
28. Yerbury, J.J.; Stewart, E.M.; Wyatt, A.R.; Wilson, M.R. Quality control of protein folding in extracellular space. *EMBO Rep.* **2005**, *6*, 1131–1136. [[CrossRef](#)]
29. Chevet, E.; Cameron, P.H.; Pelletier, M.F.; Thomas, D.Y.; Bergeron, J.J. The endoplasmic reticulum: Integration of protein folding, quality control, signaling and degradation. *Curr. Opin. Struct. Biol.* **2001**, *11*, 120–124. [[CrossRef](#)]
30. Stefani, M. Protein aggregation diseases: Toxicity of soluble prefibrillar aggregates and their clinical significance. *Methods Mol. Biol.* **2010**, *648*, 25–41. [[CrossRef](#)]
31. Nevone, A.; Merlini, G.; Nuvolone, M. Treating Protein Misfolding Diseases: Therapeutic Successes Against Systemic Amyloidoses. *Front. Pharm.* **2020**, *11*, 1024. [[CrossRef](#)] [[PubMed](#)]
32. Howie, A.J. Origins of a pervasive, erroneous idea: The "green birefringence" of Congo red-stained amyloid. *Int. J. Exp. Pathol.* **2019**, *100*, 208–221. [[CrossRef](#)] [[PubMed](#)]
33. Howie, A.J.; Brewer, D.B.; Howell, D.; Jones, A.P. Physical basis of colors seen in Congo red-stained amyloid in polarized light. *Lab. Invest.* **2008**, *88*, 232–242. [[CrossRef](#)] [[PubMed](#)]
34. Saeed, S.M.; Fine, G. Thioflavin-T for amyloid detection. *Am. J. Clin. Pathol.* **1967**, *47*, 588–593. [[CrossRef](#)]
35. Rogers, D.R. Screening for Amyloid with the Thioflavin-T Fluorescent Method. *Am. J. Clin. Pathol.* **1965**, *44*, 59–61. [[CrossRef](#)]

36. LeVine, H., 3rd. Quantification of beta-sheet amyloid fibril structures with thioflavin T. *Methods Enzymol.* **1999**, *309*, 274–284. [[CrossRef](#)]
37. Naiki, H.; Higuchi, K.; Hosokawa, M.; Takeda, T. Fluorometric determination of amyloid fibrils in vitro using the fluorescent dye, thioflavin T1. *Anal. Biochem.* **1989**, *177*, 244–249. [[CrossRef](#)]
38. Chatani, E.; Yuzu, K.; Ohhashi, Y.; Goto, Y. Current Understanding of the Structure, Stability and Dynamic Properties of Amyloid Fibrils. *Int J. Mol. Sci.* **2021**, *22*, 4349. [[CrossRef](#)]
39. Sipe, J.D.; Benson, M.D.; Buxbaum, J.N.; Ikeda, S.I.; Merlini, G.; Saraiva, M.J.; Westermark, P. Amyloid fibril proteins and amyloidosis: Chemical identification and clinical classification International Society of Amyloidosis 2016 Nomenclature Guidelines. *Amyloid* **2016**, *23*, 209–213. [[CrossRef](#)]
40. Vaxman, I.; Gertz, M. Recent Advances in the Diagnosis, Risk Stratification, and Management of Systemic Light-Chain Amyloidosis. *Acta. Haematol.* **2019**, *141*, 93–106. [[CrossRef](#)]
41. Fotiou, D.; Dimopoulos, M.A.; Kastiritis, E. Systemic AL Amyloidosis: Current Approaches to Diagnosis and Management. *Hemasphere* **2020**, *4*, e454. [[CrossRef](#)] [[PubMed](#)]
42. Kyle, R.A.; Larson, D.R.; Kurtin, P.J.; Kumar, S.; Cerhan, J.R.; Therneau, T.M.; Rajkumar, S.V.; Vachon, C.M.; Dispenzieri, A. Incidence of AL Amyloidosis in Olmsted County, Minnesota, 1990 through 2015. *Mayo Clin. Proc.* **2019**, *94*, 465–471. [[CrossRef](#)] [[PubMed](#)]
43. Desport, E.; Bridoux, F.; Sirac, C.; Delbes, S.; Bender, S.; Fernandez, B.; Quillard, N.; Lacombe, C.; Goujon, J.M.; Lavergne, D.; et al. AL Amyloidosis. *Orphanet. J. Rare Dis.* **2012**, *7*, 54. [[CrossRef](#)] [[PubMed](#)]
44. Weber, N.; Mollee, P.; Augustson, B.; Brown, R.; Catley, L.; Gibson, J.; Harrison, S.; Ho, P.J.; Horvath, N.; Jaksic, W.; et al. Management of systemic AL amyloidosis: Recommendations of the Myeloma Foundation of Australia Medical and Scientific Advisory Group. *Intern. Med. J.* **2015**, *45*, 371–382. [[CrossRef](#)] [[PubMed](#)]
45. Elsayed, M.; Usher, S.; Habib, M.H.; Ahmed, N.; Ali, J.; Begemann, M.; Shabbir, S.A.; Shune, L.; Al-Hilli, J.; Cossor, F.; et al. Current Updates on the Management of AL Amyloidosis. *J. Hematol.* **2020**, *10*, 147–161. [[CrossRef](#)]
46. Quock, T.P.; Yan, T.; Chang, E.; Guthrie, S.; Broder, M.S. Epidemiology of AL amyloidosis: A real-world study using US claims data. *Blood Adv.* **2018**, *2*, 1046–1053. [[CrossRef](#)]
47. Bork, P.; Holm, L.; Sander, C. The immunoglobulin fold. Structural classification, sequence patterns and common core. *J. Mol. Biol.* **1994**, *242*, 309–320. [[CrossRef](#)]
48. Eulitz, M.; Murphy, C.; Weiss, D.T.; Solomon, A. Serologic and chemical differentiation of human lambda III light chain variable regions. *J. Immunol.* **1991**, *146*, 3091–3096.
49. Bentley, D.L.; Rabbitts, T.H. Evolution of immunoglobulin V genes: Evidence indicating that recently duplicated human V kappa sequences have diverged by gene conversion. *Cell* **1983**, *32*, 181–189. [[CrossRef](#)]
50. Retter, I.; Althaus, H.H.; Munch, R.; Muller, W. VBASE2, an integrative V gene database. *Nucleic Acids Res.* **2005**, *33*, D671–D674. [[CrossRef](#)]
51. Giudicelli, V.; Chaume, D.; Lefranc, M.P. IMGT/GENE-DB: A comprehensive database for human and mouse immunoglobulin and T cell receptor genes. *Nucleic Acids Res.* **2005**, *33*, D256–D261. [[CrossRef](#)] [[PubMed](#)]
52. Merlini, G.; Stone, M.J. Dangerous small B-cell clones. *Blood* **2006**, *108*, 2520–2530. [[CrossRef](#)] [[PubMed](#)]
53. Palladini, G.; Milani, P.; Merlini, G. Management of AL amyloidosis in 2020. *Hematol. Am. Soc. Hematol. Educ. Program.* **2020**, *2020*, 363–371. [[CrossRef](#)] [[PubMed](#)]
54. Bellotti, V.; Mangione, P.; Merlini, G. Review: Immunoglobulin light chain amyloidosis—The archetype of structural and pathogenic variability. *J. Struct. Biol.* **2000**, *130*, 280–289. [[CrossRef](#)]
55. Rennella, E.; Morgan, G.J.; Kelly, J.W.; Kay, L.E. Role of domain interactions in the aggregation of full-length immunoglobulin light chains. *Proc. Natl. Acad. Sci. USA* **2019**, *116*, 854–863. [[CrossRef](#)]
56. Desikan, K.R.; Dhodapkar, M.V.; Hough, A.; Waldron, T.; Jagannath, S.; Siegel, D.; Barlogie, B.; Tricot, G. Incidence and impact of light chain associated (AL) amyloidosis on the prognosis of patients with multiple myeloma treated with autologous transplantation. *Leuk Lymphoma* **1997**, *27*, 315–319. [[CrossRef](#)]
57. Xu, J.; Wang, M.; Shen, Y.; Yan, M.; Xie, W.; Wang, B.; Liu, H.; Cen, X. Effects of Amyloid Light-Chain Amyloidosis on Clinical Characteristics and Prognosis in Multiple Myeloma: A Single-Center Retrospective Study. *Cancer. Manag. Res.* **2021**, *13*, 1343–1356. [[CrossRef](#)]
58. Del Pozo-Yauner, L.B.; Becerril, B.; Ochoa-Leyva, L.; Rodríguez-Ambriz, S.L.; Pérez Carrión, J.I.; Zavala-Padilla, G.; Sánchez-López, R.; Fernández Velasco, D.A. The structural determinants of the immunoglobulin light chain amyloid aggregation. In *Physical Biology of Proteins and Peptides*; Olivares-Quiroz, L.G.-L.O., Jardón-Valadez, H., Eds.; Springer: Cham, Switzerland, 2015; pp. 1–28.
59. Herrera, G.A.; Teng, J.; Turbat-Herrera, E.A.; Zeng, C.; Del Pozo-Yauner, L. Understanding Mesangial Pathobiology in AL-Amyloidosis and Monoclonal Ig Light Chain Deposition Disease. *Kidney Int. Rep.* **2020**, *5*, 1870–1893. [[CrossRef](#)]
60. Davis, D.P.; Gallo, G.; Vogen, S.M.; Dul, J.L.; Sciarretta, K.L.; Kumar, A.; Raffen, R.; Stevens, F.J.; Argon, Y. Both the environment and somatic mutations govern the aggregation pathway of pathogenic immunoglobulin light chain. *J. Mol. Biol.* **2001**, *313*, 1021–1034. [[CrossRef](#)]
61. Fandrich, M.; Dobson, C.M. The behaviour of polyamino acids reveals an inverse side chain effect in amyloid structure formation. *EMBO J.* **2002**, *21*, 5682–5690. [[CrossRef](#)]

62. Iconomidou, V.A.; Chryssikos, G.D.; Gionis, V.; Galanis, A.S.; Cordopatis, P.; Hoenger, A.; Hamodrakas, S.J. Amyloid fibril formation propensity is inherent into the hexapeptide tandemly repeating sequence of the central domain of silkworm chorion proteins of the A-family. *J. Struct. Biol.* **2006**, *156*, 480–488. [[CrossRef](#)] [[PubMed](#)]
63. Reches, M.; Gazit, E. Amyloidogenic hexapeptide fragment of medin: Homology to functional islet amyloid polypeptide fragments. *Amyloid* **2004**, *11*, 81–89. [[CrossRef](#)] [[PubMed](#)]
64. Tenidis, K.; Waldner, M.; Bernhagen, J.; Fischle, W.; Bergmann, M.; Weber, M.; Merkle, M.L.; Voelter, W.; Brunner, H.; Kapurniotu, A. Identification of a penta- and hexapeptide of islet amyloid polypeptide (IAPP) with amyloidogenic and cytotoxic properties. *J. Mol. Biol.* **2000**, *295*, 1055–1071. [[CrossRef](#)] [[PubMed](#)]
65. Fandrich, M. On the structural definition of amyloid fibrils and other polypeptide aggregates. *Cell Mol. Life Sci.* **2007**, *64*, 2066–2078. [[CrossRef](#)]
66. Sabate, R.; Espargaro, A.; de Groot, N.S.; Valle-Delgado, J.J.; Fernandez-Busquets, X.; Ventura, S. The role of protein sequence and amino acid composition in amyloid formation: Scrambling and backward reading of IAPP amyloid fibrils. *J. Mol. Biol.* **2010**, *404*, 337–352. [[CrossRef](#)]
67. Lopez de la Paz, M.; Serrano, L. Sequence determinants of amyloid fibril formation. *Proc. Natl. Acad. Sci. USA* **2004**, *101*, 87–92. [[CrossRef](#)]
68. Maurer-Stroh, S.; Debulpaep, M.; Kuemmerer, N.; Lopez de la Paz, M.; Martins, I.C.; Reumers, J.; Morris, K.L.; Copland, A.; Serpell, L.; Serrano, L.; et al. Exploring the sequence determinants of amyloid structure using position-specific scoring matrices. *Nat. Methods* **2010**, *7*, 237–242. [[CrossRef](#)]
69. Esteras-Chopo, A.; Serrano, L.; Lopez de la Paz, M. The amyloid stretch hypothesis: Recruiting proteins toward the dark side. *Proc. Natl. Acad. Sci. USA* **2005**, *102*, 16672–16677. [[CrossRef](#)]
70. Ventura, S.; Zurdo, J.; Narayanan, S.; Parreno, M.; Mangues, R.; Reif, B.; Chiti, F.; Giannoni, E.; Dobson, C.M.; Aviles, F.X.; et al. Short amino acid stretches can mediate amyloid formation in globular proteins: The Src homology 3 (SH3) case. *Proc. Natl. Acad. Sci. USA* **2004**, *101*, 7258–7263. [[CrossRef](#)]
71. Teng, P.K.; Eisenberg, D. Short protein segments can drive a non-fibrillizing protein into the amyloid state. *Protein Eng. Des. Sel.* **2009**, *22*, 531–536. [[CrossRef](#)]
72. Pastor, M.T.; Esteras-Chopo, A.; Serrano, L. Hacking the code of amyloid formation: The amyloid stretch hypothesis. *Prion* **2007**, *1*, 9–14. [[CrossRef](#)] [[PubMed](#)]
73. Makin, O.S.; Atkins, E.; Sikorski, P.; Johansson, J.; Serpell, L.C. Molecular basis for amyloid fibril formation and stability. *Proc. Natl. Acad. Sci. USA* **2005**, *102*, 315–320. [[CrossRef](#)] [[PubMed](#)]
74. Wiltzius, J.J.; Sievers, S.A.; Sawaya, M.R.; Cascio, D.; Popov, D.; Riek, C.; Eisenberg, D. Atomic structure of the cross-beta spine of islet amyloid polypeptide (amylin). *Protein Sci.* **2008**, *17*, 1467–1474. [[CrossRef](#)] [[PubMed](#)]
75. Ruiz-Zamora, R.A.; Guillaume, S.; Al-Hilaly, Y.K.; Al-Garawi, Z.; Rodriguez-Alvarez, F.J.; Zavala-Padilla, G.; Perez-Carreón, J.I.; Rodriguez-Ambríz, S.L.; Herrera, G.A.; Becerril-Lujan, B.; et al. The CDR1 and Other Regions of Immunoglobulin Light Chains are Hot Spots for Amyloid Aggregation. *Sci. Rep.* **2019**, *9*, 3123. [[CrossRef](#)]
76. Sawaya, M.R.; Sambashivan, S.; Nelson, R.; Ivanova, M.I.; Sievers, S.A.; Apostol, M.I.; Thompson, M.J.; Balbirnie, M.; Wiltzius, J.J.; McFarlane, H.T.; et al. Atomic structures of amyloid cross-beta spines reveal varied steric zippers. *Nature* **2007**, *447*, 453–457. [[CrossRef](#)]
77. Perchiacca, J.M.; Ladiwala, A.R.; Bhattacharya, M.; Tessier, P.M. Structure-based design of conformation- and sequence-specific antibodies against amyloid beta. *Proc. Natl. Acad. Sci. USA* **2012**, *109*, 84–89. [[CrossRef](#)]
78. Cheng, L.; Zhang, J.; Li, X.Y.; Yuan, L.; Pan, Y.F.; Chen, X.R.; Gao, T.M.; Qiao, J.T.; Qi, J.S. A novel antibody targeting sequence 31–35 in amyloid beta protein attenuates Alzheimer’s disease-related neuronal damage. *Hippocampus* **2017**, *27*, 122–133. [[CrossRef](#)]
79. Poduslo, J.F.; Curran, G.L.; Kumar, A.; Frangione, B.; Soto, C. Beta-sheet breaker peptide inhibitor of Alzheimer’s amyloidogenesis with increased blood-brain barrier permeability and resistance to proteolytic degradation in plasma. *J. Neurobiol.* **1999**, *39*, 371–382. [[CrossRef](#)]
80. Thompson, M.J.; Sievers, S.A.; Karanicolas, J.; Ivanova, M.I.; Baker, D.; Eisenberg, D. The 3D profile method for identifying fibril-forming segments of proteins. *Proc. Natl. Acad. Sci. USA* **2006**, *103*, 4074–4078. [[CrossRef](#)]
81. Brumshtein, B.; Esswein, S.R.; Sawaya, M.R.; Rosenberg, G.; Ly, A.T.; Landau, M.; Eisenberg, D.S. Identification of two principal amyloid-driving segments in variable domains of Ig light chains in systemic light-chain amyloidosis. *J. Biol. Chem.* **2018**, *293*, 19659–19671. [[CrossRef](#)]
82. Schmidt, A.; Annamalai, K.; Schmidt, M.; Grigorieff, N.; Fandrich, M. Cryo-EM reveals the steric zipper structure of a light chain-derived amyloid fibril. *Proc. Natl. Acad. Sci. USA* **2016**, *113*, 6200–6205. [[CrossRef](#)] [[PubMed](#)]
83. Del Pozo Yauner, L.; Ortiz, E.; Sanchez, R.; Sanchez-Lopez, R.; Guereca, L.; Murphy, C.L.; Allen, A.; Wall, J.S.; Fernandez-Velasco, D.A.; Solomon, A.; et al. Influence of the germline sequence on the thermodynamic stability and fibrillogenicity of human lambda 6 light chains. *Proteins* **2008**, *72*, 684–692. [[CrossRef](#)] [[PubMed](#)]
84. Belli, M.; Ramazzotti, M.; Chiti, F. Prediction of amyloid aggregation in vivo. *EMBO Rep.* **2011**, *12*, 657–663. [[CrossRef](#)] [[PubMed](#)]
85. Swuec, P.; Lavatelli, F.; Tasaki, M.; Paisonni, C.; Rognoni, P.; Maritan, M.; Brambilla, F.; Milani, P.; Mauri, P.; Camilloni, C.; et al. Cryo-EM structure of cardiac amyloid fibrils from an immunoglobulin light chain AL amyloidosis patient. *Nat. Commun.* **2019**, *10*, 1269. [[CrossRef](#)]

86. Hu, L.; Cui, W.; He, Z.; Shi, X.; Feng, K.; Ma, B.; Cai, Y.D. Cooperativity among short amyloid stretches in long amyloidogenic sequences. *PLoS ONE* **2012**, *7*, e39369. [[CrossRef](#)] [[PubMed](#)]
87. Lecoq, L.; Wiegand, T.; Rodriguez-Alvarez, F.J.; Cadalbert, R.; Herrera, G.A.; Del Pozo-Yauner, L.; Meier, B.H.; Bockmann, A. A Substantial Structural Conversion of the Native Monomer Leads to in-Register Parallel Amyloid Fibril Formation in Light-Chain Amyloidosis. *Chembiochem* **2019**, *20*, 1027–1031. [[CrossRef](#)]
88. Hurler, M.R.; Helms, L.R.; Li, L.; Chan, W.; Wetzel, R. A role for destabilizing amino acid replacements in light-chain amyloidosis. *Proc. Natl. Acad. Sci. USA* **1994**, *91*, 5446–5450. [[CrossRef](#)]
89. Helms, L.R.; Wetzel, R. Specificity of abnormal assembly in immunoglobulin light chain deposition disease and amyloidosis. *J. Mol. Biol.* **1996**, *257*, 77–86. [[CrossRef](#)]
90. Wetzel, R. Domain stability in immunoglobulin light chain deposition disorders. *Adv. Protein Chem.* **1997**, *50*, 183–242. [[CrossRef](#)]
91. Kim, Y.S.; Cape, S.P.; Chi, E.; Raffin, R.; Wilkins-Stevens, P.; Stevens, F.J.; Manning, M.C.; Randolph, T.W.; Solomon, A.; Carpenter, J.F. Counteracting effects of renal solutes on amyloid fibril formation by immunoglobulin light chains. *J. Biol. Chem.* **2001**, *276*, 1626–1633. [[CrossRef](#)]
92. Blancas-Mejia, L.M.; Hammernik, J.; Marin-Argany, M.; Ramirez-Alvarado, M. Differential effects on light chain amyloid formation depend on mutations and type of glycosaminoglycans. *J. Biol. Chem.* **2015**, *290*, 4953–4965. [[CrossRef](#)] [[PubMed](#)]
93. Blancas-Mejia, L.M.; Tischer, A.; Thompson, J.R.; Tai, J.; Wang, L.; Auton, M.; Ramirez-Alvarado, M. Kinetic control in protein folding for light chain amyloidosis and the differential effects of somatic mutations. *J. Mol. Biol.* **2014**, *426*, 347–361. [[CrossRef](#)] [[PubMed](#)]
94. Del Pozo-Yauner, L.; Wall, J.S.; Gonzalez Andrade, M.; Sanchez-Lopez, R.; Rodriguez-Ambriz, S.L.; Perez Carreon, J.I.; Ochoa-Leyva, A.; Fernandez-Velasco, D.A. The N-terminal strand modulates immunoglobulin light chain fibrillogenesis. *Biochem. Biophys. Res. Commun.* **2014**, *443*, 495–499. [[CrossRef](#)] [[PubMed](#)]
95. Gonzalez-Andrade, M.; Becerril-Lujan, B.; Sanchez-Lopez, R.; Cecena-Alvarez, H.; Perez-Carreón, J.I.; Ortiz, E.; Fernandez-Velasco, D.A.; del Pozo-Yauner, L. Mutational and genetic determinants of lambda6 light chain amyloidogenesis. *FEBS J.* **2013**, *280*, 6173–6183. [[CrossRef](#)] [[PubMed](#)]
96. Kim, Y.; Wall, J.S.; Meyer, J.; Murphy, C.; Randolph, T.W.; Manning, M.C.; Solomon, A.; Carpenter, J.F. Thermodynamic modulation of light chain amyloid fibril formation. *J. Biol. Chem.* **2000**, *275*, 1570–1574. [[CrossRef](#)]
97. Marin-Argany, M.; Guell-Bosch, J.; Blancas-Mejia, L.M.; Villegas, S.; Ramirez-Alvarado, M. Mutations can cause light chains to be too stable or too unstable to form amyloid fibrils. *Protein Sci.* **2015**, *24*, 1829–1840. [[CrossRef](#)]
98. Poshusta, T.L.; Sikkink, L.A.; Leung, N.; Clark, R.J.; Dispenzieri, A.; Ramirez-Alvarado, M. Mutations in specific structural regions of immunoglobulin light chains are associated with free light chain levels in patients with AL amyloidosis. *PLoS ONE* **2009**, *4*, e5169. [[CrossRef](#)]
99. Sikkink, L.A.; Ramirez-Alvarado, M. Biochemical and aggregation analysis of Bence Jones proteins from different light chain diseases. *Amyloid* **2008**, *15*, 29–39. [[CrossRef](#)]
100. Wall, J.S.; Gupta, V.; Wilkerson, M.; Schell, M.; Loris, R.; Adams, P.; Solomon, A.; Stevens, F.; Dealwis, C. Structural basis of light chain amyloidogenicity: Comparison of the thermodynamic properties, fibrillogenic potential and tertiary structural features of four Vlambda6 proteins. *J. Mol. Recognit.* **2004**, *17*, 323–331. [[CrossRef](#)]
101. Blancas-Mejia, L.M.; Tellez, L.A.; del Pozo-Yauner, L.; Becerril, B.; Sanchez-Ruiz, J.M.; Fernandez-Velasco, D.A. Thermodynamic and kinetic characterization of a germ line human lambda6 light-chain protein: The relation between unfolding and fibrillogenesis. *J. Mol. Biol.* **2009**, *386*, 1153–1166. [[CrossRef](#)]
102. Wall, J.; Schell, M.; Murphy, C.; Hrcic, R.; Stevens, F.J.; Solomon, A. Thermodynamic instability of human lambda 6 light chains: Correlation with fibrillogenicity. *Biochemistry* **1999**, *38*, 14101–14108. [[CrossRef](#)] [[PubMed](#)]
103. Ramirez-Alvarado, M.; Merkel, J.S.; Regan, L. A systematic exploration of the influence of the protein stability on amyloid fibril formation in vitro. *Proc. Natl. Acad. Sci. USA* **2000**, *97*, 8979–8984. [[CrossRef](#)] [[PubMed](#)]
104. Qin, Z.; Hu, D.; Zhu, M.; Fink, A.L. Structural characterization of the partially folded intermediates of an immunoglobulin light chain leading to amyloid fibrillation and amorphous aggregation. *Biochemistry* **2007**, *46*, 3521–3531. [[CrossRef](#)] [[PubMed](#)]
105. Misra, P.; Ramirez-Alvarado, M. Early events in light chain aggregation at physiological pH reveal new insights on assembly, stability, and aggregate dissociation. *Amyloid* **2021**, *28*, 113–124. [[CrossRef](#)]
106. Rottenaicher, G.J.; Weber, B.; Ruhrnoss, F.; Kazman, P.; Absmeier, R.M.; Hitzemberger, M.; Zacharias, M.; Buchner, J. Molecular mechanism of amyloidogenic mutations in hypervariable regions of antibody light chains. *J. Biol. Chem.* **2021**, *296*, 100334. [[CrossRef](#)]
107. Garay Sanchez, S.A.; Rodriguez Alvarez, F.J.; Zavala-Padilla, G.; Mejia-Cristobal, L.M.; Cruz-Rangel, A.; Costas, M.; Fernandez Velasco, D.A.; Melendez-Zajgla, J.; Del Pozo-Yauner, L. Stability and aggregation propensity do not fully account for the association of various germline variable domain gene segments with light chain amyloidosis. *Biol. Chem.* **2017**, *398*, 477–489. [[CrossRef](#)]
108. Baden, E.M.; Owen, B.A.; Peterson, F.C.; Volkman, B.F.; Ramirez-Alvarado, M.; Thompson, J.R. Altered dimer interface decreases stability in an amyloidogenic protein. *J. Biol. Chem.* **2008**, *283*, 15853–15860. [[CrossRef](#)] [[PubMed](#)]
109. Baden, E.M.; Randles, E.G.; Aboagye, A.K.; Thompson, J.R.; Ramirez-Alvarado, M. Structural insights into the role of mutations in amyloidogenesis. *J. Biol. Chem.* **2008**, *283*, 30950–30956. [[CrossRef](#)]

110. Peterson, F.C.; Baden, E.M.; Owen, B.A.; Volkman, B.F.; Ramirez-Alvarado, M. A single mutation promotes amyloidogenicity through a highly promiscuous dimer interface. *Structure* **2010**, *18*, 563–570. [[CrossRef](#)]
111. Nawata, M.; Tsutsumi, H.; Kobayashi, Y.; Unzai, S.; Mine, S.; Nakamura, T.; Uegaki, K.; Kamikubo, H.; Kataoka, M.; Hamada, D. Heat-induced native dimerization prevents amyloid formation by variable domain from immunoglobulin light-chain REI. *FEBS J.* **2017**, *284*, 3114–3127. [[CrossRef](#)]
112. Mukherjee, S.; Pondaven, S.P.; Hand, K.; Madine, J.; Jaroniec, C.P. Effect of amino acid mutations on the conformational dynamics of amyloidogenic immunoglobulin light-chains: A combined NMR and in silico study. *Sci. Rep.* **2017**, *7*, 10339. [[CrossRef](#)]
113. Peterle, D.; Klimtchuk, E.S.; Wales, T.E.; Georgescauld, F.; Connors, L.H.; Engen, J.R.; Gursky, O. A Conservative Point Mutation in a Dynamic Antigen-binding Loop of Human Immunoglobulin lambda6 Light Chain Promotes Pathologic Amyloid Formation. *J. Mol. Biol.* **2021**, *433*, 167310. [[CrossRef](#)] [[PubMed](#)]
114. Kazman, P.; Vielberg, M.T.; Pulido Cendales, M.D.; Hunzinger, L.; Weber, B.; Hegenbart, U.; Zacharias, M.; Kohler, R.; Schonland, S.; Groll, M.; et al. Fatal amyloid formation in a patient's antibody light chain is caused by a single point mutation. *eLife* **2020**, *9*, e52300. [[CrossRef](#)] [[PubMed](#)]
115. Bodi, K.; Prokaeva, T.; Spencer, B.; Eberhard, M.; Connors, L.H.; Seldin, D.C. AL-Base: A visual platform analysis tool for the study of amyloidogenic immunoglobulin light chain sequences. *Amyloid* **2009**, *16*, 1–8. [[CrossRef](#)] [[PubMed](#)]
116. Kyle, R.A.; Gertz, M.A. Primary systemic amyloidosis: Clinical and laboratory features in 474 cases. *Semin. Hematol.* **1995**, *32*, 45–59.
117. Solomon, A.; Frangione, B.; Franklin, E.C. Bence Jones proteins and light chains of immunoglobulins. Preferential association of the V lambda VI subgroup of human light chains with amyloidosis AL (lambda). *J. Clin. Investig.* **1982**, *70*, 453–460. [[CrossRef](#)] [[PubMed](#)]
118. Ozaki, S.; Abe, M.; Wolfenbarger, D.; Weiss, D.T.; Solomon, A. Preferential expression of human lambda-light-chain variable-region subgroups in multiple myeloma, AL amyloidosis, and Waldenstrom's macroglobulinemia. *Clin. Immunol. Immunopathol.* **1994**, *71*, 183–189. [[CrossRef](#)]
119. Abraham, R.S.; Geyer, S.M.; Price-Troska, T.L.; Allmer, C.; Kyle, R.A.; Gertz, M.A.; Fonseca, R. Immunoglobulin light chain variable (V) region genes influence clinical presentation and outcome in light chain-associated amyloidosis (AL). *Blood* **2003**, *101*, 3801–3808. [[CrossRef](#)] [[PubMed](#)]
120. Comenzo, R.L.; Wally, J.; Kica, G.; Murray, J.; Ericsson, T.; Skinner, M.; Zhang, Y. Clonal immunoglobulin light chain variable region germline gene use in AL amyloidosis: Association with dominant amyloid-related organ involvement and survival after stem cell transplantation. *Br. J. Haematol.* **1999**, *106*, 744–751. [[CrossRef](#)]
121. Kourelis, T.V.; Dasari, S.; Theis, J.D.; Ramirez-Alvarado, M.; Kurtin, P.J.; Gertz, M.A.; Zeldenrust, S.R.; Zenka, R.M.; Dogan, A.; Dispenzieri, A. Clarifying immunoglobulin gene usage in systemic and localized immunoglobulin light-chain amyloidosis by mass spectrometry. *Blood* **2017**, *129*, 299–306. [[CrossRef](#)]
122. Perfetti, V.; Casarini, S.; Palladini, G.; Vignarelli, M.C.; Klersy, C.; Diegoli, M.; Ascari, E.; Merlini, G. Analysis of V(lambda)-J(lambda) expression in plasma cells from primary (AL) amyloidosis and normal bone marrow identifies 3r (lambdaIII) as a new amyloid-associated germline gene segment. *Blood* **2002**, *100*, 948–953. [[CrossRef](#)] [[PubMed](#)]
123. Pokkuluri, P.R.; Solomon, A.; Weiss, D.T.; Stevens, F.J.; Schiffer, M. Tertiary structure of human lambda 6 light chains. *Amyloid* **1999**, *6*, 165–171. [[CrossRef](#)] [[PubMed](#)]
124. Sidana, S.; Dasari, S.; Kourelis, T.V.; Dispenzieri, A.; Murray, D.L.; King, R.L.; McPhail, E.D.; Ramirez-Alvarado, M.; Kumar, S.K.; Gertz, M.A. IGVL gene region usage correlates with distinct clinical presentation in IgM vs non-IgM light chain amyloidosis. *Blood Adv.* **2021**, *5*, 2101–2105. [[CrossRef](#)] [[PubMed](#)]
125. Comenzo, R.L.; Zhang, Y.; Martinez, C.; Osman, K.; Herrera, G.A. The tropism of organ involvement in primary systemic amyloidosis: Contributions of Ig V(L) germ line gene use and clonal plasma cell burden. *Blood* **2001**, *98*, 714–720. [[CrossRef](#)] [[PubMed](#)]
126. Richardson, J.S.; Getzoff, E.D.; Richardson, D.C. The beta bulge: A common small unit of nonrepetitive protein structure. *Proc. Natl. Acad. Sci. USA* **1978**, *75*, 2574–2578. [[CrossRef](#)]
127. Hernandez-Santoyo, A.; del Pozo Yauner, L.; Fuentes-Silva, D.; Ortiz, E.; Rudino-Pinera, E.; Sanchez-Lopez, R.; Horjales, E.; Becerril, B.; Rodriguez-Romero, A. A single mutation at the sheet switch region results in conformational changes favoring lambda6 light-chain fibrillogenesis. *J. Mol. Biol.* **2010**, *396*, 280–292. [[CrossRef](#)]
128. Radamaker, L.; Karimi-Farsijani, S.; Andreotti, G.; Baur, J.; Neumann, M.; Schreiner, S.; Berghaus, N.; Motika, R.; Haupt, C.; Walther, P.; et al. Role of mutations and post-translational modifications in systemic AL amyloidosis studied by cryo-EM. *Nat. Commun.* **2021**, *12*, 6434. [[CrossRef](#)]
129. Ehrnhoefer, D.E.; Sutton, L.; Hayden, M.R. Small changes, big impact: Posttranslational modifications and function of huntingtin in Huntington disease. *Neuroscientist* **2011**, *17*, 475–492. [[CrossRef](#)]
130. Lu, Y.; Jiang, Y.; Prokaeva, T.; Connors, L.H.; Costello, C.E. Oxidative Post-Translational Modifications of an Amyloidogenic Immunoglobulin Light Chain Protein. *Int. J. Mass Spectrom.* **2017**, *416*, 71–79. [[CrossRef](#)]
131. Zottig, X.; Laporte Wolwertz, M.; Golizeh, M.; Ohlund, L.; Sleno, L.; Bourgault, S. Effects of oxidative post-translational modifications on structural stability and self-assembly of lambda6 immunoglobulin light chain. *Biophys. Chem.* **2016**, *219*, 59–68. [[CrossRef](#)]

132. Souillac, P.O.; Uversky, V.N.; Millett, I.S.; Khurana, R.; Doniach, S.; Fink, A.L. Elucidation of the molecular mechanism during the early events in immunoglobulin light chain amyloid fibrillation. Evidence for an off-pathway oligomer at acidic pH. *J. Biol. Chem.* **2002**, *277*, 12666–12679. [[CrossRef](#)] [[PubMed](#)]
133. Velazquez-Lopez, I.; Valdes-Garcia, G.; Romero Romero, S.; Maya Martinez, R.; Leal-Cervantes, A.I.; Costas, M.; Sanchez-Lopez, R.; Amero, C.; Pastor, N.; Fernandez Velasco, D.A. Localized conformational changes trigger the pH-induced fibrillogenesis of an amyloidogenic lambda light chain protein. *Biochim. Biophys. Acta. Gen. Subj.* **2018**, *1862*, 1656–1666. [[CrossRef](#)] [[PubMed](#)]
134. Epstein, W.V.; Tan, M.; Wood, I.S. Formation of "amyloid" fibrils in vitro by action of human kidney lysosomal enzymes on Bence Jones proteins. *J. Lab. Clin. Med.* **1974**, *84*, 107–110.
135. Mukherjee, S.; Pondaven, S.P.; Jaroniec, C.P. Conformational flexibility of a human immunoglobulin light chain variable domain by relaxation dispersion nuclear magnetic resonance spectroscopy: Implications for protein misfolding and amyloid assembly. *Biochemistry* **2011**, *50*, 5845–5857. [[CrossRef](#)] [[PubMed](#)]
136. Tzotzos, S.; Doig, A.J. Amyloidogenic sequences in native protein structures. *Protein Sci.* **2010**, *19*, 327–348. [[CrossRef](#)]
137. Del Pozo Yauner, L.; Ortiz, E.; Becerril, B. The CDR1 of the human lambdaVI light chains adopts a new canonical structure. *Proteins* **2006**, *62*, 122–129. [[CrossRef](#)] [[PubMed](#)]
138. Solomon, A.; Weiss, D.T.; Williams, T.K. Experimental model of human light-chain-associated disease. *Curr. Top. Microbiol. Immunol.* **1992**, *182*, 261–267. [[CrossRef](#)]
139. Stevens, P.W.; Raffin, R.; Hanson, D.K.; Deng, Y.L.; Berrios-Hammond, M.; Westholm, F.A.; Murphy, C.; Eulitz, M.; Wetzel, R.; Solomon, A.; et al. Recombinant immunoglobulin variable domains generated from synthetic genes provide a system for in vitro characterization of light-chain amyloid proteins. *Protein Sci.* **1995**, *4*, 421–432. [[CrossRef](#)]
140. Maya-Martinez, R.; French-Pacheco, L.; Valdes-Garcia, G.; Pastor, N.; Amero, C. Different Dynamics in 6aJL2 Proteins Associated with AL Amyloidosis, a Conformational Disease. *Int. J. Mol. Sci.* **2019**, *20*, 3078. [[CrossRef](#)]
141. Maya-Martinez, R.; Gil-Rodriguez, P.; Amero, C. Solution structure of 6aJL2 and 6aJL2-R24G amyloidogenic light chain proteins. *Biochem. Biophys. Res. Commun.* **2015**, *456*, 695–699. [[CrossRef](#)]
142. Pelaez-Aguilar, A.E.; Valdes-Garcia, G.; French-Pacheco, L.; Pastor, N.; Amero, C.; Rivillas-Acevedo, L. Site-Specific Interactions with Copper Promote Amyloid Fibril Formation for lambda6aJL2-R24G. *ACS Omega* **2020**, *5*, 7085–7095. [[CrossRef](#)]
143. Valdes-Garcia, G.; Millan-Pacheco, C.; Pastor, N. Convergent mechanisms favor fast amyloid formation in two lambda 6a Ig light chain mutants. *Biopolymers* **2017**, *107*, e23027. [[CrossRef](#)] [[PubMed](#)]
144. Khurana, R.; Gillespie, J.R.; Talapatra, A.; Minert, L.J.; Ionescu-Zanetti, C.; Millett, I.; Fink, A.L. Partially folded intermediates as critical precursors of light chain amyloid fibrils and amorphous aggregates. *Biochemistry* **2001**, *40*, 3525–3535. [[CrossRef](#)] [[PubMed](#)]
145. Klimtchuk, E.S.; Gursky, O.; Patel, R.S.; Laporte, K.L.; Connors, L.H.; Skinner, M.; Seldin, D.C. The critical role of the constant region in thermal stability and aggregation of amyloidogenic immunoglobulin light chain. *Biochemistry* **2010**, *49*, 9848–9857. [[CrossRef](#)] [[PubMed](#)]
146. Morgan, G.J.; Kelly, J.W. The Kinetic Stability of a Full-Length Antibody Light Chain Dimer Determines whether Endoproteolysis Can Release Amyloidogenic Variable Domains. *J. Mol. Biol.* **2016**, *428*, 4280–4297. [[CrossRef](#)] [[PubMed](#)]
147. Blancas-Mejia, L.M.; Martin, E.B.; Williams, A.; Wall, J.S.; Ramirez-Alvarado, M. Kinetic stability and sequence/structure studies of urine-derived Bence-Jones proteins from multiple myeloma and light chain amyloidosis patients. *Biophys. Chem.* **2017**, *230*, 89–98. [[CrossRef](#)] [[PubMed](#)]
148. Glenner, G.G.; Ein, D.; Eanes, E.D.; Bladen, H.A.; Terry, W.; Page, D.L. Creation of "amyloid" fibrils from Bence Jones proteins in vitro. *Science* **1971**, *174*, 712–714. [[CrossRef](#)]
149. Linke, R.P.; Tischendorf, F.W.; Zucker-Franklin, D.; Franklin, E.C. The formation of amyloid-like fibrils in vitro from Bence Jones Proteins of the VLambdaI subclass. *J. Immunol.* **1973**, *111*, 24–26.
150. Rocken, C.; Hegenbarth, V.; Schmitz, M.; Stix, B.; Schade, G.; Mohnert, A.; Roessner, A. Plasmacytoma of the tonsil with AL amyloidosis: Evidence of post-fibrillogenic proteolysis of the fibril protein. *Virchows Arch.* **2000**, *436*, 336–344. [[CrossRef](#)]
151. Enqvist, S.; Sletten, K.; Westermarck, P. Fibril protein fragmentation pattern in systemic AL-amyloidosis. *J. Pathol.* **2009**, *219*, 473–480. [[CrossRef](#)]
152. Lavatelli, F.; Mazzini, G.; Ricagno, S.; Iavarone, F.; Rognoni, P.; Milani, P.; Nuvolone, M.; Swuec, P.; Caminito, S.; Tasaki, M.; et al. Mass spectrometry characterization of light chain fragmentation sites in cardiac AL amyloidosis: Insights into the timing of proteolysis. *J. Biol. Chem.* **2020**, *295*, 16572–16584. [[CrossRef](#)] [[PubMed](#)]
153. Mazzini, G.; Ricagno, S.; Caminito, S.; Rognoni, P.; Milani, P.; Nuvolone, M.; Basset, M.; Foli, A.; Russo, R.; Merlini, G.; et al. Protease-sensitive regions in amyloid light chains: What a common pattern of fragmentation across organs suggests about aggregation. *FEBS J.* **2021**, *289*, 494–506. [[CrossRef](#)] [[PubMed](#)]
154. Stevens, F.J.; Kisilevsky, R. Immunoglobulin light chains, glycosaminoglycans, and amyloid. *Cell Mol. Life Sci.* **2000**, *57*, 441–449. [[CrossRef](#)] [[PubMed](#)]
155. Nieva, J.; Shafton, A.; Altobelli, L.J., 3rd; Tripuraneni, S.; Rogel, J.K.; Wentworth, A.D.; Lerner, R.A.; Wentworth, P., Jr. Lipid-derived aldehydes accelerate light chain amyloid and amorphous aggregation. *Biochemistry* **2008**, *47*, 7695–7705. [[CrossRef](#)]
156. Herrera, G.A.; Del Pozo-Yauner, L.; Teng, J.; Zeng, C.; Shen, X.; Moriyama, T.; Ramirez Alcantara, V.; Liu, B.; Turbat-Herrera, E.A. Glomerulopathic Light Chain-Mesangial Cell Interactions: Sortilin-Related Receptor (SORL1) and Signaling. *Kidney Int. Rep.* **2021**, *6*, 1379–1396. [[CrossRef](#)]

157. McLaughlin, R.W.; De Stigter, J.K.; Sikkink, L.A.; Baden, E.M.; Ramirez-Alvarado, M. The effects of sodium sulfate, glycosaminoglycans, and Congo red on the structure, stability, and amyloid formation of an immunoglobulin light-chain protein. *Protein Sci.* **2006**, *15*, 1710–1722. [[CrossRef](#)]
158. Ren, R.; Hong, Z.; Gong, H.; Laporte, K.; Skinner, M.; Seldin, D.C.; Costello, C.E.; Connors, L.H.; Trinkaus-Randall, V. Role of glycosaminoglycan sulfation in the formation of immunoglobulin light chain amyloid oligomers and fibrils. *J. Biol. Chem.* **2010**, *285*, 37672–37682. [[CrossRef](#)]
159. Murphy, R.M. Kinetics of amyloid formation and membrane interaction with amyloidogenic proteins. *Biochim. Biophys. Acta* **2007**, *1768*, 1923–1934. [[CrossRef](#)]
160. Marin-Argany, M.; Lin, Y.; Misra, P.; Williams, A.; Wall, J.S.; Howell, K.G.; Elsbernd, L.R.; McClure, M.; Ramirez-Alvarado, M. Cell Damage in Light Chain Amyloidosis: Fibril internalization, toxicity and cell-mediated seeding. *J. Biol. Chem.* **2016**, *291*, 19813–19825. [[CrossRef](#)]
161. Makin, O.S.; Serpell, L.C. Examining the structure of the mature amyloid fibril. *Biochem. Soc. Trans.* **2002**, *30*, 521–525. [[CrossRef](#)]
162. Eanes, E.D.; Glenner, G.G. X-ray diffraction studies on amyloid filaments. *J. Histochem. Cytochem.* **1968**, *16*, 673–677. [[CrossRef](#)] [[PubMed](#)]
163. Fitzpatrick, A.W.; Debelouchina, G.T.; Bayro, M.J.; Clare, D.K.; Caporini, M.A.; Bajaj, V.S.; Jaroniec, C.P.; Wang, L.; Ladizhansky, V.; Muller, S.A.; et al. Atomic structure and hierarchical assembly of a cross-beta amyloid fibril. *Proc. Natl. Acad. Sci. USA* **2013**, *110*, 5468–5473. [[CrossRef](#)] [[PubMed](#)]
164. Almeida, Z.L.; Brito, R.M.M. Structure and Aggregation Mechanisms in Amyloids. *Molecules* **2020**, *25*, 1195. [[CrossRef](#)] [[PubMed](#)]
165. Schormann, N.; Murrell, J.R.; Liepnieks, J.J.; Benson, M.D. Tertiary structure of an amyloid immunoglobulin light chain protein: A proposed model for amyloid fibril formation. *Proc. Natl. Acad. Sci. USA* **1995**, *92*, 9490–9494. [[CrossRef](#)]
166. Serpell, L.C.; Sunde, M.; Benson, M.D.; Tennent, G.A.; Pepys, M.B.; Fraser, P.E. The protofilament substructure of amyloid fibrils. *J. Mol. Biol.* **2000**, *300*, 1033–1039. [[CrossRef](#)]
167. Khurana, R.; Ionescu-Zanetti, C.; Pope, M.; Li, J.; Nielson, L.; Ramirez-Alvarado, M.; Regan, L.; Fink, A.L.; Carter, S.A. A general model for amyloid fibril assembly based on morphological studies using atomic force microscopy. *Biophys. J.* **2003**, *85*, 1135–1144. [[CrossRef](#)]
168. Radamaker, L.; Lin, Y.H.; Annamalai, K.; Huhn, S.; Hegenbart, U.; Schonland, S.O.; Fritz, G.; Schmidt, M.; Fandrich, M. Cryo-EM structure of a light chain-derived amyloid fibril from a patient with systemic AL amyloidosis. *Nat. Commun.* **2019**, *10*, 1103. [[CrossRef](#)]
169. Radamaker, L.; Baur, J.; Huhn, S.; Haupt, C.; Hegenbart, U.; Schonland, S.; Bansal, A.; Schmidt, M.; Fandrich, M. Cryo-EM reveals structural breaks in a patient-derived amyloid fibril from systemic AL amyloidosis. *Nat. Commun.* **2021**, *12*, 875. [[CrossRef](#)]
170. Piehl, D.W.; Blancas-Mejia, L.M.; Ramirez-Alvarado, M.; Rienstra, C.M. Solid-state NMR chemical shift assignments for AL-09 VL immunoglobulin light chain fibrils. *Biomol. NMR Assign.* **2017**, *11*, 45–50. [[CrossRef](#)]
171. Pradhan, T.; Annamalai, K.; Sarkar, R.; Hegenbart, U.; Schonland, S.; Fandrich, M.; Reif, B. Solid state NMR assignments of a human lambda-III immunoglobulin light chain amyloid fibril. *Biomol. NMR Assign.* **2021**, *15*, 9–16. [[CrossRef](#)]
172. Pradhan, T.; Annamalai, K.; Sarkar, R.; Huhn, S.; Hegenbart, U.; Schonland, S.; Fandrich, M.; Reif, B. Seeded fibrils of the germline variant of human lambda-III immunoglobulin light chain FOR005 have a similar core as patient fibrils with reduced stability. *J. Biol. Chem.* **2020**, *295*, 18474–18484. [[CrossRef](#)] [[PubMed](#)]
173. Hora, M.; Sarkar, R.; Morris, V.; Xue, K.; Prade, E.; Harding, E.; Buchner, J.; Reif, B. MAK33 antibody light chain amyloid fibrils are similar to oligomeric precursors. *PLoS ONE* **2017**, *12*, e0181799. [[CrossRef](#)] [[PubMed](#)]
174. Piehl, D.W.; Blancas-Mejia, L.M.; Wall, J.S.; Kennel, S.J.; Ramirez-Alvarado, M.; Rienstra, C.M. Immunoglobulin Light Chains Form an Extensive and Highly Ordered Fibril Involving the N- and C-Termini. *ACS Omega* **2017**, *2*, 712–720. [[CrossRef](#)] [[PubMed](#)]
175. Gutierrez-Gonzalez, L.H.; Muresanu, L.; del Pozo-Yauner, L.; Sanchez, R.; Guereca, L.; Becerril, B.; Lucke, C. (1)H, (13)C and (15)N resonance assignment of 6aJL2(R25G), a highly fibrillogenic lambdaVI light chain variable domain. *Biomol. NMR Assign.* **2007**, *1*, 159–161. [[CrossRef](#)] [[PubMed](#)]
176. Rudino-Pinera, E.; Pelaez-Aguilar, A.E.; Amero, C.; Diaz-Vilchis, A. Crystal structure of 6aJL2-R24G light chain variable domain: Does crystal packing explain amyloid fibril formation? *Biochem. Biophys. Rep.* **2019**, *20*, 100682. [[CrossRef](#)]
177. Honda, R.; Kuwata, K. Evidence for a central role of PrP helix 2 in the nucleation of amyloid fibrils. *FASEB J.* **2018**, *32*, 3641–3652. [[CrossRef](#)]
178. Townsend, D.; Hughes, E.; Hussain, R.; Siligardi, G.; Baldock, S.; Madine, J.; Middleton, D.A. Heparin and Methionine Oxidation Promote the Formation of Apolipoprotein A-I Amyloid Comprising alpha-Helical and beta-Sheet Structures. *Biochemistry* **2017**, *56*, 1632–1644. [[CrossRef](#)]
179. Chen, Y.C. Impact of a discordant helix on beta-amyloid structure, aggregation ability and toxicity. *Eur. Biophys. J.* **2017**, *46*, 681–687. [[CrossRef](#)]
180. Lo, C.J.; Wang, C.C.; Huang, H.B.; Chang, C.F.; Shiao, M.S.; Chen, Y.C.; Lin, T.H. The Arctic mutation accelerates Abeta aggregation in SDS through reducing the helical propensity of residues 15–25. *Amyloid* **2015**, *22*, 8–18. [[CrossRef](#)]
181. Berhanu, W.M.; Alred, E.J.; Hansmann, U.H. Stability of Osaka Mutant and Wild-Type Fibril Models. *J. Phys. Chem. B* **2015**, *119*, 13063–13070. [[CrossRef](#)]
182. Grasso, G.; Leanza, L.; Morbiducci, U.; Danani, A.; Deriu, M.A. Aminoacid substitutions in the glycine zipper affect the conformational stability of amyloid beta fibrils. *J. Biomol. Struct. Dyn.* **2020**, *38*, 3908–3915. [[CrossRef](#)] [[PubMed](#)]

183. O’Nuallain, B.; Shivaprasad, S.; Kheterpal, I.; Wetzel, R. Thermodynamics of A beta(1-40) amyloid fibril elongation. *Biochemistry* **2005**, *44*, 12709–12718. [[CrossRef](#)] [[PubMed](#)]
184. Abe, Y.; Shibata, H.; Oyama, K.; Ueda, T. Effect of O-glycosylation on amyloid fibril formation of the variable domain in the Vlambda6 light chain mutant Wil. *Int J. Biol. Macromol.* **2021**, *166*, 342–351. [[CrossRef](#)] [[PubMed](#)]
185. Omtvedt, L.A.; Bailey, D.; Renouf, D.V.; Davies, M.J.; Paramonov, N.A.; Haavik, S.; Husby, G.; Sletten, K.; Hounsell, E.F. Glycosylation of immunoglobulin light chains associated with amyloidosis. *Amyloid* **2000**, *7*, 227–244. [[CrossRef](#)] [[PubMed](#)]
186. Kumar, S.; Murray, D.; Dasari, S.; Milani, P.; Barnidge, D.; Madden, B.; Kourelis, T.; Arendt, B.; Merlini, G.; Ramirez-Alvarado, M.; et al. Assay to rapidly screen for immunoglobulin light chain glycosylation: A potential path to earlier AL diagnosis for a subset of patients. *Leukemia* **2019**, *33*, 254–257. [[CrossRef](#)] [[PubMed](#)]
187. Jordan, T.L.; Maar, K.; Redhage, K.R.; Misra, P.; Blancas-Mejia, L.M.; Dick, C.J.; Wall, J.S.; Williams, A.; Dietz, A.B.; van Wijnen, A.J.; et al. Light chain amyloidosis induced inflammatory changes in cardiomyocytes and adipose-derived mesenchymal stromal cells. *Leukemia* **2020**, *34*, 1383–1393. [[CrossRef](#)] [[PubMed](#)]
188. McWilliams-Koeppe, H.P.; Foster, J.S.; Hackenbrack, N.; Ramirez-Alvarado, M.; Donohoe, D.; Williams, A.; Macy, S.; Wooliver, C.; Wortham, D.; Morrell-Falvey, J.; et al. Light Chain Amyloid Fibrils Cause Metabolic Dysfunction in Human Cardiomyocytes. *PLoS ONE* **2015**, *10*, e0137716. [[CrossRef](#)]
189. Shi, J.; Guan, J.; Jiang, B.; Brenner, D.A.; Del Monte, F.; Ward, J.E.; Connors, L.H.; Sawyer, D.B.; Semigran, M.J.; Macgillivray, T.E.; et al. Amyloidogenic light chains induce cardiomyocyte contractile dysfunction and apoptosis via a non-canonical p38alpha MAPK pathway. *Proc. Natl. Acad. Sci. USA* **2010**, *107*, 4188–4193. [[CrossRef](#)]
190. Brenner, D.A.; Jain, M.; Pimentel, D.R.; Wang, B.; Connors, L.H.; Skinner, M.; Apstein, C.S.; Liao, R. Human amyloidogenic light chains directly impair cardiomyocyte function through an increase in cellular oxidant stress. *Circ. Res.* **2004**, *94*, 1008–1010. [[CrossRef](#)]
191. Martin, D.J.; Ramirez-Alvarado, M. Glycosaminoglycans promote fibril formation by amyloidogenic immunoglobulin light chains through a transient interaction. *Biophys. Chem.* **2011**, *158*, 81–89. [[CrossRef](#)]
192. Alexandrescu, A.T. Amyloid accomplices and enforcers. *Protein Sci.* **2005**, *14*, 1–12. [[CrossRef](#)] [[PubMed](#)]
193. Luna-Martinez, O.D.; Hernandez-Santoyo, A.; Villalba-Velazquez, M.I.; Sanchez-Alcala, R.; Fernandez-Velasco, D.A.; Becerril, B. Stabilizing an amyloidogenic lambda6 light chain variable domain. *FEBS J.* **2017**, *284*, 3702–3717. [[CrossRef](#)] [[PubMed](#)]
194. Abe, M.; Abe, Y.; Ohkuri, T.; Mishima, T.; Monji, A.; Kanba, S.; Ueda, T. Mechanism for retardation of amyloid fibril formation by sugars in Vlambda6 protein. *Protein Sci.* **2013**, *22*, 467–474. [[CrossRef](#)] [[PubMed](#)]
195. Mishima, T.; Ohkuri, T.; Monji, A.; Kanemaru, T.; Abe, Y.; Ueda, T. Residual structures in the acid-unfolded states of Vlambda6 proteins affect amyloid fibrillation. *J. Mol. Biol.* **2009**, *392*, 1033–1043. [[CrossRef](#)] [[PubMed](#)]
196. Kazman, P.; Absmeier, R.M.; Engelhardt, H.; Buchner, J. Dissection of the amyloid formation pathway in AL amyloidosis. *Nat. Commun.* **2021**, *12*, 6516. [[CrossRef](#)] [[PubMed](#)]
197. Brumshtein, B.; Esswein, S.R.; Salwinski, L.; Phillips, M.L.; Ly, A.T.; Cascio, D.; Sawaya, M.R.; Eisenberg, D.S. Inhibition by small-molecule ligands of formation of amyloid fibrils of an immunoglobulin light chain variable domain. *eLife* **2015**, *4*, e10935. [[CrossRef](#)]
198. Wolwertz, M.L.; Nguyen, P.T.; Quittot, N.; Bourgault, S. Probing the role of lambda6 immunoglobulin light chain dimerization in amyloid formation. *Biochim. Biophys. Acta* **2016**, *1864*, 409–418. [[CrossRef](#)] [[PubMed](#)]
199. Arosio, P.; Owczarz, M.; Muller-Spath, T.; Rognoni, P.; Beeg, M.; Wu, H.; Salmona, M.; Morbidelli, M. In vitro aggregation behavior of a non-amyloidogenic lambda light chain dimer deriving from U266 multiple myeloma cells. *PLoS ONE* **2012**, *7*, e33372. [[CrossRef](#)]
200. Myatt, E.A.; Westholm, F.A.; Weiss, D.T.; Solomon, A.; Schiffer, M.; Stevens, F.J. Pathogenic potential of human monoclonal immunoglobulin light chains: Relationship of in vitro aggregation to in vivo organ deposition. *Proc. Natl. Acad. Sci. USA* **1994**, *91*, 3034–3038. [[CrossRef](#)]
201. Thompson, A.J.; Barrow, C.J. Protein conformational misfolding and amyloid formation: Characteristics of a new class of disorders that include Alzheimer’s and Prion diseases. *Curr. Med. Chem.* **2002**, *9*, 1751–1762. [[CrossRef](#)]
202. Chiti, F.; Dobson, C.M. Protein misfolding, functional amyloid, and human disease. *Annu. Rev. Biochem.* **2006**, *75*, 333–366. [[CrossRef](#)] [[PubMed](#)]
203. Nilsson, M.R. Techniques to study amyloid fibril formation in vitro. *Methods* **2004**, *34*, 151–160. [[CrossRef](#)] [[PubMed](#)]
204. Chiti, F.; Webster, P.; Taddei, N.; Clark, A.; Stefani, M.; Ramponi, G.; Dobson, C.M. Designing conditions for in vitro formation of amyloid protofilaments and fibrils. *Proc. Natl. Acad. Sci. USA* **1999**, *96*, 3590–3594. [[CrossRef](#)]
205. Bonifacio, M.J.; Sakaki, Y.; Saraiva, M.J. ‘In vitro’ amyloid fibril formation from transthyretin: The influence of ions and the amyloidogenicity of TTR variants. *Biochim. Biophys. Acta* **1996**, *1316*, 35–42. [[CrossRef](#)]
206. Janciauskiene, S.; Carlemalm, E.; Eriksson, S. In vitro amyloid fibril formation from alpha 1-antitrypsin. *Biol. Chem. Hoppe Seyler* **1995**, *376*, 103–109. [[CrossRef](#)]
207. Klafki, H.W.; Pick, A.I.; Pardowitz, I.; Cole, T.; Awni, L.A.; Barnikol, H.U.; Mayer, F.; Kratzin, H.D.; Hilschmann, N. Reduction of disulfide bonds in an amyloidogenic Bence Jones protein leads to formation of “amyloid-like” fibrils in vitro. *Biol. Chem. Hoppe Seyler* **1993**, *374*, 1117–1122. [[CrossRef](#)]
208. Colon, W.; Kelly, J.W. Partial denaturation of transthyretin is sufficient for amyloid fibril formation in vitro. *Biochemistry* **1992**, *31*, 8654–8660. [[CrossRef](#)]

209. Connors, L.H.; Shirahama, T.; Skinner, M.; Fenves, A.; Cohen, A.S. In vitro formation of amyloid fibrils from intact beta 2-microglobulin. *Biochem. Biophys. Res. Commun.* **1985**, *131*, 1063–1068. [[CrossRef](#)]
210. Bucciantini, M.; Rigacci, S.; Stefani, M. Amyloid Aggregation: Role of Biological Membranes and the Aggregate-Membrane System. *J. Phys. Chem. Lett.* **2014**, *5*, 517–527. [[CrossRef](#)]
211. Husby, G.; Stenstad, T.; Magnus, J.H.; Sletten, K.; Nordvag, B.Y.; Marhaug, G. Interaction between circulating amyloid fibril protein precursors and extracellular tissue matrix components in the pathogenesis of systemic amyloidosis. *Clin. Immunol. Immunopathol.* **1994**, *70*, 2–9. [[CrossRef](#)]
212. Keeling, J.; Teng, J.; Herrera, G.A. AL-amyloidosis and light-chain deposition disease light chains induce divergent phenotypic transformations of human mesangial cells. *Lab. Investig.* **2004**, *84*, 1322–1338. [[CrossRef](#)] [[PubMed](#)]
213. Sousa, M.M.; do Amaral, J.B.; Guimaraes, A.; Saraiva, M.J. Up-regulation of the extracellular matrix remodeling genes, biglycan, neutrophil gelatinase-associated lipocalin, and matrix metalloproteinase-9 in familial amyloid polyneuropathy. *FASEB J.* **2005**, *19*, 124–126. [[CrossRef](#)] [[PubMed](#)]
214. Vora, M.; Kevil, C.G.; Herrera, G.A. Contribution of human smooth muscle cells to amyloid angiopathy in AL (light-chain) amyloidosis. *Ultrastruct Pathol.* **2017**, *41*, 358–368. [[CrossRef](#)] [[PubMed](#)]
215. Zhang, X.; Chen, J.; Wang, S. Serum Amyloid A Induces a Vascular Smooth Muscle Cell Phenotype Switch through the p38 MAPK Signaling Pathway. *Biomed. Res. Int.* **2017**, *2017*, 4941379. [[CrossRef](#)] [[PubMed](#)]
216. Khvotchev, M.; Sudhof, T.C. Proteolytic processing of amyloid-beta precursor protein by secretases does not require cell surface transport. *J. Biol. Chem.* **2004**, *279*, 47101–47108. [[CrossRef](#)]
217. Fisher, Y.; Nemirovsky, A.; Baron, R.; Monsonogo, A. Dendritic cells regulate amyloid-beta-specific T-cell entry into the brain: The role of perivascular amyloid-beta. *J. Alzheimers Dis.* **2011**, *27*, 99–111. [[CrossRef](#)]
218. Domert, J.; Rao, S.B.; Agholme, L.; Brorsson, A.C.; Marcusson, J.; Hallbeck, M.; Nath, S. Spreading of amyloid-beta peptides via neuritic cell-to-cell transfer is dependent on insufficient cellular clearance. *Neurobiol. Dis.* **2014**, *65*, 82–92. [[CrossRef](#)]
219. Shirahama, T.; Cohen, A.S. Intralysosomal formation of amyloid fibrils. *Am. J. Pathol.* **1975**, *81*, 101–116.
220. Shirahama, T.; Cohen, A.S. An analysis of the close relationship of lysosomes to early deposits of amyloid. Ultrastructural evidence in experimental mouse amyloidosis. *Am. J. Pathol.* **1973**, *73*, 97–114.
221. Shirahama, T.; Cohen, A.S. Lysosomal breakdown of amyloid fibrils by macrophages. *Am. J. Pathol.* **1971**, *63*, 463–486.
222. Kluge-Beckerman, B.; Manaloor, J.J.; Liepnieks, J.J. A pulse-chase study tracking the conversion of macrophage-endocytosed serum amyloid A into extracellular amyloid. *Arthritis Rheum.* **2002**, *46*, 1905–1913. [[CrossRef](#)] [[PubMed](#)]
223. Russell, W.J.; Cardelli, J.; Harris, E.; Baier, R.J.; Herrera, G.A. Monoclonal light chain-mesangial cell interactions: Early signaling events and subsequent pathologic effects. *Lab. Investig.* **2001**, *81*, 689–703. [[CrossRef](#)] [[PubMed](#)]
224. Solomon, A.; Weiss, D.T.; Schell, M.; Hrcic, R.; Murphy, C.L.; Wall, J.; McGavin, M.D.; Pan, H.J.; Kabalka, G.W.; Paulus, M.J. Transgenic mouse model of AA amyloidosis. *Am. J. Pathol.* **1999**, *154*, 1267–1272. [[CrossRef](#)]
225. Tagouri, Y.M.; Sanders, P.W.; Picken, M.M.; Siegal, G.P.; Kerby, J.D.; Herrera, G.A. In vitro AL-amyloid formation by rat and human mesangial cells. *Lab Investig.* **1996**, *74*, 290–302.
226. Christensen, E.I.; Birn, H. Megalin and cubilin: Synergistic endocytic receptors in renal proximal tubule. *Am. J. Physiol. Ren. Physiol.* **2001**, *280*, F562–F573. [[CrossRef](#)]
227. Verroust, P.J.; Christensen, E.I. Megalin and cubilin—The story of two multipurpose receptors unfolds. *Nephrol Dial. Transpl.* **2002**, *17*, 1867–1871. [[CrossRef](#)]
228. Herrera, G.A. Plasticity of mesangial cells: A basis for understanding pathological alterations. *Ultrastruct Pathol.* **2006**, *30*, 471–479. [[CrossRef](#)]
229. Keeling, J.; Herrera, G.A. Matrix metalloproteinases and mesangial remodeling in light chain-related glomerular damage. *Kidney Int.* **2005**, *68*, 1590–1603. [[CrossRef](#)]
230. Teng, J.; Turbat-Herrera, E.A.; Herrera, G.A. Extrusion of amyloid fibrils to the extracellular space in experimental mesangial AL-amyloidosis: Transmission and scanning electron microscopy studies and correlation with renal biopsy observations. *Ultrastruct Pathol.* **2014**, *38*, 104–115. [[CrossRef](#)]
231. Teng, J.; Russell, W.J.; Gu, X.; Cardelli, J.; Jones, M.L.; Herrera, G.A. Different types of glomerulopathic light chains interact with mesangial cells using a common receptor but exhibit different intracellular trafficking patterns. *Lab. Investig.* **2004**, *84*, 440–451. [[CrossRef](#)]
232. Teng, J.; Turbat-Herrera, E.A.; Herrera, G.A. Role of translational research advancing the understanding of the pathogenesis of light chain-mediated glomerulopathies. *Pathol Int.* **2007**, *57*, 398–412. [[CrossRef](#)] [[PubMed](#)]
233. Isaac, J.; Kerby, J.D.; Russell, W.J.; Dempsey, S.C.; Sanders, P.W.; Herrera, G.A. In vitro modulation of AL-amyloid formation by human mesangial cells exposed to amyloidogenic light chains. *Amyloid* **1998**, *5*, 238–246. [[CrossRef](#)] [[PubMed](#)]
234. Hu, X.; Crick, S.L.; Bu, G.; Frieden, C.; Pappu, R.V.; Lee, J.M. Amyloid seeds formed by cellular uptake, concentration, and aggregation of the amyloid-beta peptide. *Proc. Natl. Acad. Sci. USA* **2009**, *106*, 20324–20329. [[CrossRef](#)] [[PubMed](#)]
235. Herrera, G.A.; Teng, J.; Zeng, C.; Xu, H.; Liang, M.; Alexander, J.S.; Liu, B.; Boyer, C.; Turbat-Herrera, E.A. Phenotypic plasticity of mesenchymal stem cells is crucial for mesangial repair in a model of immunoglobulin light chain-associated mesangial damage. *Ultrastruct Pathol.* **2018**, *42*, 262–288. [[CrossRef](#)] [[PubMed](#)]
236. Verma, M.; Vats, A.; Taneja, V. Toxic species in amyloid disorders: Oligomers or mature fibrils. *Ann. Indian Acad. Neurol.* **2015**, *18*, 138–145. [[CrossRef](#)]

237. Wong, C.Y.; Cheong, S.K.; Mok, P.L.; Leong, C.F. Differentiation of human mesenchymal stem cells into mesangial cells in post-glomerular injury murine model. *Pathology* **2008**, *40*, 52–57. [[CrossRef](#)]
238. Wong, C.Y.; Tan, E.L.; Cheong, S.K. In vitro differentiation of mesenchymal stem cells into mesangial cells when co-cultured with injured mesangial cells. *Cell Biol. Int.* **2014**, *38*, 497–501. [[CrossRef](#)]
239. Kisilevsky, R. Amyloids: Tombstones or triggers? *Nat. Med.* **2000**, *6*, 633–634. [[CrossRef](#)]
240. Absmeier, R.M.; Rottenaicher, G.J.; Svilenov, H.L.; Kazman, P.; Buchner, J. Antibodies gone bad - the molecular mechanism of light chain amyloidosis. *FEBS J.* **2022**. [[CrossRef](#)]
241. Otzen, D.E. Driving forces in amyloidosis: How does a light chain make a heavy heart? *J. Biol. Chem.* **2021**, *296*, 100785. [[CrossRef](#)]